Article

TRANSPARENT PROCESS OPEN ACCESS

EMBO reports

A GID E3 ligase assembly ubiquitinates an Rsp5 E3 adaptor and regulates plasma membrane transporters

Christine R Langlois[1,*], Viola Beier[1], Ozge Karayel[2], Jakub Chrustowicz[1], Dawafuti Sherpa[1], Matthias Mann[2] & Brenda A Schulman[1,**]

Abstract

Cells rapidly remodel their proteomes to align their cellular metabolism to environmental conditions. Ubiquitin E3 ligases enable this response, by facilitating rapid and reversible changes to protein stability, localization, or interaction partners. In *Saccharomyces cerevisiae*, the GID E3 ligase regulates the switch from gluconeogenic to glycolytic conditions through induction and incorporation of the substrate receptor subunit Gid4, which promotes the degradation of gluconeogenic enzymes. Here, we show an alternative substrate receptor, Gid10, which is induced in response to changes in temperature, osmolarity, and nutrient availability, regulates the ART-Rsp5 ubiquitin ligase pathway, a component of plasma membrane quality control. Proteomic studies reveal that the levels of the adaptor protein Art2 are elevated upon *GID10* deletion. A crystal structure shows the basis for Gid10-Art2 interactions, and we demonstrate that Gid10 directs a GID E3 ligase complex to ubiquitinate Art2. Our data suggest that the GID E3 ligase affects Art2-dependent amino acid transport. This study reveals GID as a system of E3 ligases with metabolic regulatory functions outside of glycolysis and gluconeogenesis, controlled by distinct stress-specific substrate receptors.

Keywords GID; metabolism; nutrient signaling; Rsp5; ubiquitin E3 ligase
Subject Categories Membranes & Trafficking; Post-translational Modifications & Proteolysis; Structural Biology
DOI 10.15252/embr.202153835 | Received 18 August 2021 | Revised 22 March 2022 | Accepted 30 March 2022 | Published online 19 April 2022
EMBO Reports (2022) 23: e53835

Introduction

The ubiquitin system is an integral part of cellular responses to environmental changes. The post-translational modification of proteins with ubiquitin modulates virtually every cellular pathway and all aspects of protein fate, including gene expression, and protein activity, stability, localization, and binding partners (Varshavsky, 2012). Because of their wide-reaching effects, substrate selection by E3 ubiquitin ligases must be strictly controlled to maintain cellular homeostasis upon environmental perturbations (Sui *et al*, 2020). Indeed, the cell simultaneously employs several control mechanisms to ensure faithful selection of E3 ligase substrates, but how these mechanisms are coordinated across cellular pathways remains poorly understood.

The transfer of one or more ubiquitins to substrate proteins requires a hierarchical pathway, in which ubiquitin is first activated by an E1 ubiquitin activating enzyme, and then transferred to an E2 ubiquitin conjugating enzyme, which together with an E3 ubiquitin ligase covalently attaches ubiquitin to the substrate (Cappadocia & Lima, 2018). The two largest E3 ligase families are the HECT (*H*omologous to the *E*6AP *C*arboxyl *T*erminus)-type E3 ligases, which first pass the ubiquitin from the E2 to the E3 before substrate attachment, and the RING (*R*eally *I*nteresting *N*ew *G*ene) E3 ligases, which facilitate the direct transfer of ubiquitin from the E2 to a remotely bound substrate (Deshaies & Joazeiro, 2009; Rotin & Kumar, 2009).

E3 ligases can encompass substrate binding and a catalytic HECT or RING domain all within a single subunit, or substrates can be recruited through receptor subunits. Although many HECT E3 ligases are thought to be single subunit enzymes, some members of the Nedd4 family employ adaptor proteins for substrate selection (Dupré *et al*, 2004; Foot *et al*, 2008; Lin *et al*, 2008; Mund & Pelham, 2009; Trimpert *et al*, 2017). Although constellations of WW domains in Nedd4 family E3 ligases directly recognize PYx(Y/F) motifs in some substrates, in some cases, an intervening PYx(Y/F)-containing adaptor bridges the E3 ligase and substrate (Huibregtse *et al*, 1993; Lu *et al*, 1999; Ogunjimi *et al*, 2005; Polo & Di Fiore, 2008; Persaud *et al*, 2014). Nedd4 family adaptor proteins can also modulate the E3's sub-cellular localization, which can promote ubiquitination of specific substrates while sequestering the ligase away from others (Plant *et al*, 2000; Hettema *et al*, 2004; Shearwin-Whyatt *et al*, 2006). In the budding yeast *Saccharomyces cerevisiae*, Rsp5 is the sole Nedd4 family E3 ubiquitin ligase, and its PYx(Y/F)-containing

1 Department of Molecular Machines and Signaling, Max Planck Institute of Biochemistry, Martinsried, Germany
2 Department of Proteomics and Signal Transduction, Max Planck Institute of Biochemistry, Martinsried, Germany
*Corresponding author. Tel: +49 89 85782409; E-mail: langlois@biochem.mpg.de
**Corresponding author. Tel: +49 89 85783709; E-mail: schulman@biochem.mpg.de

adaptor proteins, termed ARTs (*A*rrestin-*R*elated *T*rafficking adaptors), are best recognized for regulating endocytosis of plasma membrane nutrient transporters to serve cellular metabolic needs (Lin *et al*, 2008; Lauwers *et al*, 2010; Zhao *et al*, 2013). The ART family consists of 14 such adaptor proteins, in a complex network involving activation in response to specific environmental stimuli (Becuwe *et al*, 2012; Ivashov *et al*, 2020; Kahlhofer *et al*, 2020).

Nutrient signaling originating at the plasma membrane also simultaneously regulates cellular synthesis of metabolites. For example, in the absence of glucose, glucose transporters are rapidly endocytosed, and the cell additionally initiates transcriptional and translational programs to promote gluconeogenesis. When glucose becomes available again, cells rapidly restore glucose transporters to the plasma membrane, terminate gluconeogenesis, and resume the more energetically favorable glycolysis (Gancedo, 1998; Barnett & Entian, 2005; Hovsepian *et al*, 2017). One regulator of this response in *S. cerevisiae* is the multi-protein GID (*G*lucose *I*nduced degradation *D*eficient) E3 ligase, an N-degron E3 ligase that preferentially targets substrates with an N-terminal proline (Chen *et al*, 2017). Upon glucose availability following carbon starvation, the GID E3 ligase targets rate-limiting gluconeogenic enzymes, including fructose 1,6-bisphosphatase (Fbp1) and malate dehydrogenase (Mdh2), for degradation (Hämmerle *et al*, 1998; Santt *et al*, 2008; Chen *et al*, 2017; Qiao *et al*, 2020). Intriguingly, despite the critical function carried out by the GID complex during glycolytic growth, subunits of the GID E3 ligase are dispensable for viability and there is no characterized phenotype of GID deletions (Hämmerle *et al*, 1998). While the function of the GID E3 ligase during the switch from gluconeogenic to glycolytic conditions is relatively well-characterized, several lines of evidence suggest that the GID E3 ligase is competent to regulate additional substrates and metabolic pathways in response to a variety of stressors.

First, the GID complex forms multiple distinct assemblies *in vivo*, with each assembly promoting the targeting of discrete substrates. For example, incorporation of Gid7 into GID^{SR4} results in the formation of a supramolecular chelate assembly (Chelator-GID), uniquely suited to target the oligomeric structure of Fbp1 (Sherpa *et al*, 2021). Second, for both the Chelator assembly harboring Gid7, or singular versions without Gid7, the GID ligase is expressed as an anticipatory complex (GID^{Ant}) in virtually all growth conditions, allowing it to rapidly respond to a shift in conditions. GID^{Ant} is comprised of the scaffolding subunits Gid1, Gid5, and Gid8, as well as the RING-like domain containing subunits Gid2 and Gid9. Following a shift in environmental conditions, GID^{Ant} is activated by the binding of substrate receptor (SR) to form GID^{SR} (Santt *et al*, 2008; Menssen *et al*, 2012; Qiao *et al*, 2020). Third, GID^{Ant} can bind multiple substrate receptors, including Gid4, Gid10, and the recently identified Gid11 (Melnykov *et al*, 2019; Kong *et al*, 2021). For example, during the switch from gluconeogenic to glycolytic conditions, the substrate receptor Gid4 is induced and binds GID^{Ant}, forming the active GID^{SR4}, which in turn recruits gluconeogenic enzymes (Menssen *et al*, 2012; Chen *et al*, 2017; Qiao *et al*, 2020). In contrast, heat or osmotic shock induces the expression of Gid10 and the formation of the structurally homologous GID^{SR10} (Melnykov *et al*, 2019; Qiao *et al*, 2020), the targets of which remain unknown.

The molecular mechanisms underlying coordination of various E3 ligase pathways in response to environmental changes remain poorly understood. To explore these questions, we use the GID E3 ligase as a model multifunctional metabolic regulator. We characterize the regulation of expression of the SRs Gid4 and Gid10. Each SR is transiently induced under distinct environmental conditions, turned-over in a manner which depends on itself, and can influence binding of the other SR. Furthermore, using a mass spectrometry (MS)-based method (Karayel *et al*, 2020), we identify the ART-Rsp5 network as a novel regulatory target of GID^{SR10}, demonstrating cross-talk between the two E3 ligase pathways.

Results

Gid10 has hallmark features of a GID E3 substrate receptor *in vivo*

Previous studies implicated Gid10 as a SR of the GID E3 ligase. For example, it has been shown that both Gid4 and Gid10 bind the GID^{Ant} scaffolding subunit Gid5 (Menssen *et al*, 2012; Melnykov *et al*, 2019; Qiao *et al*, 2020). In addition, a high resolution cryo-EM structure of GID^{SR4} showed Gid4 binding a concave surface of Gid5, through key interactions mediated by its C-terminal tail, and a low resolution structure demonstrated that Gid10 forms a homologous complex (Qiao *et al*, 2020). Consistent with this, a yeast two-hybrid analysis confirmed that both Gid10 and Gid4 bind directly to Gid5 (Fig 1A). To investigate if the same intermolecular interactions are required for Gid4 and Gid10 binding, we probed the effect of structure-based mutants in the Gid5-SR binding interface. While Gid4 and Gid10 were able to bind WT GID^{Ant} to a similar extent, binding was significantly abrogated to GID^{Ant} containing Gid5 point mutations (Gid5$^{W606A,\ Y613A,\ Q649A}$) on the concave binding surface (Fig 1B), which also disrupts ubiquitination by GID^{SR4} (Qiao *et al*, 2020). Furthermore, deletion of the C-terminal residues in Gid4 or Gid10 also significantly reduced the binding of each SR to GID^{Ant} (Fig 1B), indicating that Gid4 and Gid10 bind to the same surface on Gid5 through homologous residues on each SR.

Gid4 and Gid10 share many sequence and structural elements (Appendix Fig S1) and might carry out redundant functions in the cell. Indeed, GID^{SR10} is capable of ubiquitinating Mdh2 *in vitro*, albeit to a lesser extent than GID^{SR4} (Qiao *et al*, 2020). However, Gid10 is unable to substitute for loss of Gid4 *in vivo* to promote Mdh2 or Fbp1 degradation, even when placed under the control of the Gid4 promoter (Melnykov *et al*, 2019). Because ubiquitination of Mdh2 *in vitro* by GID^{SR10} is less efficient than by GID^{SR4}, higher levels of Gid10 might be required to compensate for lack of Gid4 *in vivo*. To test this, we employed the promoter reference technique, which allows the fate of existing proteins to be monitored without the use of global transcription or translation inhibitors (Chen *et al*, 2017; Oh *et al*, 2017). During the switch between gluconeogenic and glycolytic conditions, the GID^{SR4} substrates Mdh2 and Fbp1 are significantly stabilized in a Gid4 deletion strain, but not in a Gid10 deletion strain (Figs 1C and EV1A), in agreement with previously published results (Santt *et al*, 2008; Melnykov *et al*, 2019). In addition, constitutive overexpression of Gid10 from the Tdh3 promoter alone did not significantly alter the rate of Mdh2 degradation, and could not compensate for loss of Gid4 (Fig 1C). Thus, even overexpressed Gid10 is not competent to promote recognition or degradation of Gid4 substrates during carbon recovery *in vivo*.

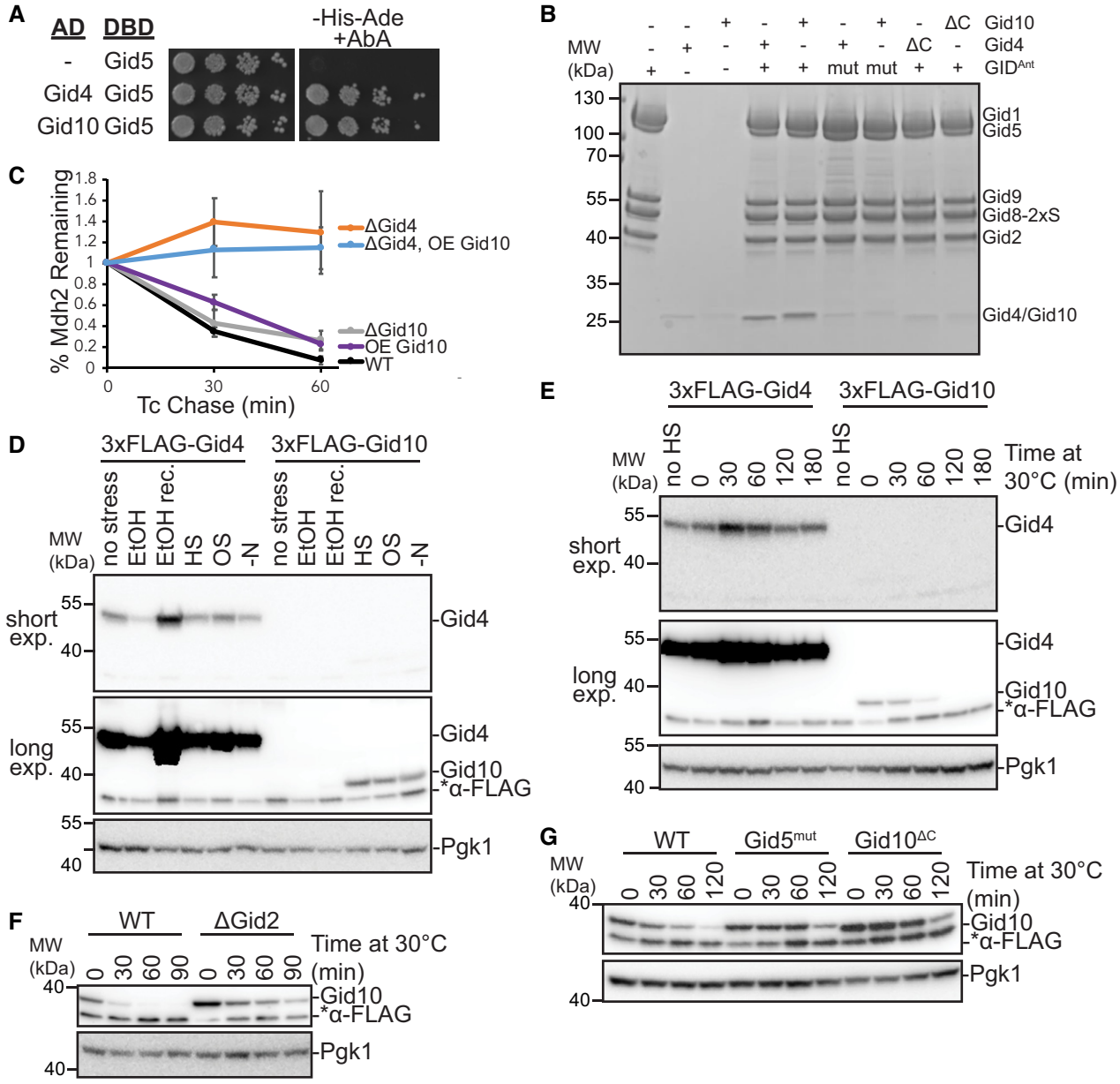

Figure 1. Gid4 and Gid10 expression is regulated by the GID E3 ligase.

A Yeast two-hybrid interactions between SR-Gal4 activation domain (AD) and Gid5-DNA binding domain (DBD). Growth on -His-Ade+Aureobasidin A (AbA) is indicative of an interaction between the two test proteins. Spots represent 1:5 serial dilutions.

B Strep-Tactin pull-down of GID^{Ant} (strep-tagged at Gid8 C-terminus) probing binding of $Gid10^{57–292}$ and $Gid4^{117–362}$ to the complex visualized with Coomassie-stained SDS-PAGE. The experiment was performed with WT and C-terminal deletion (ΔC) of the substrate receptors (Δ289–292 (FEIA) and Δ359–362 (FEFA) for Gid10 and Gid4, respectively) and WT and mutant (mut, $Gid5^{W606A/Y613A/Q649A}$) GID^{Ant}.

C Tetracycline reference-based chase performed during transition from ethanol to glucose media with wildtype, ΔGid4 and ΔGid10 strains, and in wildtype and ΔGid4 strains overexpressing (OE) Gid10. Points represent mean, error bars represent standard deviation ($n > 3$ biological replicates).

D Lysates from yeast strains expressing endogenously tagged 3xFLAG-Gid4 or 3x-FLAG-Gid10 that were grown in SD complete at 30°C (no stress), SE complete for 19 h (EtOH), SD complete for 1 h following 19 h ethanol treatment (EtOH rec.), 42°C for 1 h (HS), SD complete supplemented with 0.5 M NaCl for 1 h (OS), or SD-N for 1 h (-N) were run on an SDS-PAGE gel and immunoblotted with αFLAG (two exposures from the same gel are shown) and αPGK.

E Lysates from yeast strains expressing endogenously tagged 3xFLAG-Gid4 or 3xFLAG-Gid10 that were grown at 42°C for 1 h, and then returned to 30°C for the indicated timepoints were run on an SDS-PAGE gel and immunoblotted with αFLAG (two exposures from the same gel are shown) and αPGK.

F Lysates from wildtype and ΔGid2 yeast strains expressing endogenously tagged 3xFLAG-Gid10 that were grown at 42°C for 1 h, and then returned to 30°C for the indicated timepoints were run on an SDS-PAGE gel and immunoblotted with αFLAG and αPGK.

G Lysates from wildtype, $Gid5^{W606A,Y613A,Q649A}$ ($Gid5^{mut}$), and $Gid10^{Δ289–292}$ ($Gid10^{ΔC}$) strains expressing endogenously tagged 3xFLAG-Gid10 that were grown at 42°C for 1 h, and then returned to 30°C for the indicated timepoints were run on an SDS-PAGE gel and immunoblotted with αFLAG and αPGK.

While Gid10 protein levels are not induced during carbon starvation or recovery, they are transiently induced in response to a variety of other stress conditions, including heat shock, osmotic shock, and amino acid and nitrogen starvation (Figs 1D and EV1B–G) (Gasch *et al*, 2000; Melnykov *et al*, 2019; Qiao *et al*, 2020). Interestingly, while Gid10 is induced during heat shock, Gid4 is transiently induced during recovery from heat shock (Fig 1E), suggesting complementary roles of the two SRs during stress and recovery. To gain a better understanding of how the transient expression of SRs is regulated, we first examined the requirements of the GID complex for SR turnover. All of the subunits of GID^{Ant} were previously shown to be required for Gid4 turnover (Menssen *et al*, 2018), and thus, we hypothesized that SR degradation may be triggered after binding GID^{Ant}. Indeed, both Gid4 and Gid10 are stabilized when the RING-like containing subunit Gid2 is deleted (Figs 1F and EV1H). Furthermore, Gid4 and Gid10 are also stabilized when their ability to bind to GID^{Ant} via Gid5 is impaired (Figs 1G and EV1I), demonstrating that both GID complex activity and SR binding to GID^{Ant} are required for SR turnover.

Gid10 protein expression is significantly lower than Gid4 under all tested conditions (Fig 1D and E). Therefore, if the two SRs compete for binding to GID^{Ant} via Gid5, the absence of Gid4 should significantly affect the kinetics of Gid10 turnover, but absence of Gid10 should have little to no effect on Gid4 turnover. Indeed, Gid10 turnover during heat shock recovery is accelerated by either a deletion of Gid4 or expression of a GID^{Ant}-binding impaired Gid4 (Fig 2A). In contrast, Gid4 turnover during carbon recovery is largely unaffected by the absence of Gid10 (Fig EV1H); however, when Gid10 is constitutively overexpressed, and therefore better able to compete for GID^{Ant} binding, Gid4 turnover during recovery from carbon starvation is delayed (Fig 2B), and levels of the Gid4 substrate Fbp1 are concomitantly decreased (Fig 2C). To further investigate the ability of the two SRs to compete for binding to GID^{Ant}, we carried out an *in vitro* competition assay. In this assay, GID^{SR10} was incubated with increasing amounts of strep-tagged Gid4 and substrate receptor exchange was examined by the ability of Gid4 to co-IP with GID^{Ant}. As the amount of strep-tagged Gid4 was increased, we observed a corresponding increase in the amount of GID^{Ant} co-captured (Fig 2D). Taken together, these data are consistent with a model in which the SRs can compete with each other for access to GID^{Ant} and that binding is a prerequisite for SR turnover, suggesting that the SRs may be auto-ubiquitinated when bound to GID^{Ant}.

Art2 is a regulatory target of GID^{SR10}

Biological functions for the Gid10 protein remain elusive. To identify its regulatory targets, we employed a systems-wide single-run DIA-based proteomics approach (Karayel *et al*, 2020) during heat stress, when Gid10 is maximally expressed. This method allows quantification of differences in protein levels, and thus comparisons of yeast strains expressing or lacking Gid10 allows for the identification of potential substrates. Following a 1h heat shock at 42°C, only two proteins were significantly upregulated in a Gid10 deletion strain, compared to wild type: Art2, a member of the α-arrestin family, and Nhp10, a member of the INO80 chromatin remodeling complex ($P < 0.01$ and fold change > 4, Fig 3A) (Lu *et al*, 1996; Lussier *et al*, 1997). Importantly, regulation of both proteins was Gid10-specific as their abundance did not change in a Gid4 deletion strain (Fig 3B). To determine whether Art2 or Nhp10 might also be regulated under other growth conditions where the GID E3 ligase is known to be active, we reanalyzed our previously published data set characterizing GID-dependent protein regulation during recovery from ethanol starvation (Karayel *et al*, 2020). We selected for proteins that contain a proline in position 2 or 3, and are significantly upregulated during growth in ethanol, compared with glucose, and downregulated during recovery compared to ethanol. Interestingly, during recovery from ethanol starvation, Art2 also appears to be regulated by Gid2 (although this did not reach statistical significance), but not by Gid4 (Fig EV2A). In addition, constitutive overexpression of Gid10 during recovery from carbon starvation results in decreased levels of Art2 (Fig EV2B).

GID^{SR4} is an N-degron E3 ligase that recognizes substrates with an N-terminal proline, although peptides with other N-terminal residues have been shown to bind Gid4 or Gid10 with lower affinity (Hämmerle *et al*, 1998; Chen *et al*, 2017; Dong *et al*, 2018, 2020; Melnykov *et al*, 2019). On this basis, we probed the potential for Gid10 interaction to bind the Art2 or Nhp10 N-terminal sequences by yeast two-hybrid. Gid10 efficiently bound the Art2, but not the Nhp10, N-terminus (Figs 4A and EV3A). Moreover, the Gid10-Art2 interaction is Gid10-specific as we did not observe an interaction between Gid4 and the Art2 N-terminus (Fig 4A), and dependent on the N-terminal proline of Art2 (Fig 4B). In contrast, Gid4, but not Gid10, interacted with the N-terminus of the classic Gid4 substrate Mdh2 (Fig 4A), suggesting that Gid10 and Gid4 indeed prefer discrete regulatory targets.

To further confirm Gid10 binding to the Art2 N-terminus, we quantified the interaction using isothermal titration calorimetry. The putative Gid10 substrate-binding domain ($Gid10^{\Delta 1-56}$) bound the first 9 amino acids of Art2 (PFITSRPVA) synthesized with a C-terminal tryptophan to enable concentration determination based on extinction coefficient at 280 nm, with a K_D of 1.03 μM (Fig 4C). Notably, this is 2-fold higher affinity than any published peptide examined for interaction with Gid4 (Dong *et al*, 2018, 2020).

To determine the molecular mechanism of this interaction, we determined a crystal structure showing degron recognition by Gid10. A co-crystal structure of $Gid10^{\Delta 1-56}$ bound to a peptide corresponding to the first seven residues of Art2 (PFITSRP, plus a tryptophan at the C-terminus) showed that Gid10 resembles Gid4 in forming a β-barrel with several helical insertions (Fig 4D). In addition, the binding pocket residues on Gid4 and Gid10, the trajectory of the Fbp1 or Art2 degron in the Gid4 or Gid10 binding pocket, respectively, and the position of the N-terminal proline were strikingly similar (Fig EV3B and C). The structures of the two SRs are nearly identical, with an RMSD of 0.87 Å (Fig EV3B). However, Gid10's interaction with the Art2 sequence is far more extensive than Gid4 interactions with the Fbp1 degron in the context of Chelator-GID^{SR4}, or human Gid4 bound to Pro/N-degron peptides (Dong *et al*, 2018; Sherpa *et al*, 2021). All seven residues of the Art2 peptide interact with Gid10, explaining the relatively high affinity of this interaction.

To further characterize Art2 as a GID^{SR10} substrate, we asked if Gid^{SR10} was capable of ubiquitinating Art2. Towards this end, we performed ubiquitination assays using Art2-3xFLAG immunocaptured from yeast lysates, and recombinantly expressed GID^{Ant}, GID^{SR10}, or GID^{SR4}. In this system, GID^{SR10}, but not GID^{SR4} or GID^{Ant}, was able to efficiently poly-ubiquitinate Art2. In contrast,

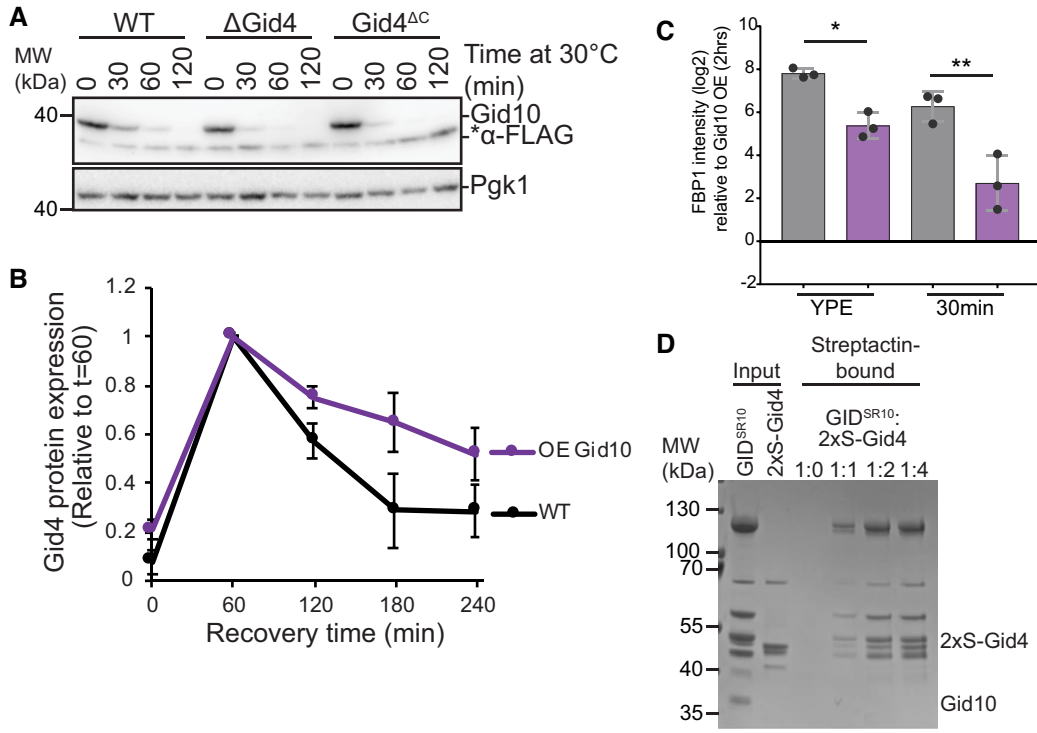

Figure 2. Gid4 and Gid10 compete for binding to GID^{Ant}.

A Lysates from wildtype, ΔGid4, and Gid4$^{\Delta C}$ strains expressing endogenously tagged 3xFLAG-Gid10 that were grown at 42°C for 1 h, and then returned to 30°C for the indicated timepoints were run on an SDS-PAGE gel and immunoblotted with αFLAG and αPGK.

B Wildtype and Gid10 overexpressing yeast strains expressing endogenously tagged Gid4 were grown for 19 h in YPE, and transitioned to YPD for the indicated timepoints. Lysates were run on an SDS-PAGE gel and immunoblotted with αFLAG and αPGK. Points represent mean, error bars represent standard deviation ($n > 3$ biological replicates).

C Fbp1 protein abundance in wildtype and Gid10 overexpressing yeast strains grown in YPE for 19 h, and following 30 min and 2 h recovery growth in YPD. Bars represent mean, error bars represent standard deviation, significance was determined by one-way ANOVA (unpaired) followed by Tukey's multiple comparison test, * indicates $P < 0.05$, ** indicates $P < 0.01$, ($n = 3$ biological replicates).

D *In vitro* competition assay probing the ability of N-terminally 2xStrep-tagged Gid4 (2xS-Gid4) to exchange with Gid10 in the GID^{SR10} complex. Proteins after Strep-Tactin pull-down were visualized by Coomassie-stained SDS-PAGE.

only GID^{SR4} was capable of ubiquitinating Mdh2 (Fig 5A and B). Moreover, GID^{SR10}-mediated ubiquitination of Art2 is dependent on Gid10 binding to Gid^{Ant}, and the ability of Art2 to bind Gid10 via its N-terminal proline (Fig 5C). Of all ubiquitin's lysines, only K48 was able to support robust poly-ubiquitination of Mdh2 by GID^{SR4} (Qiao *et al*, 2020). To test if the molecular mechanism of GID^{SR10} poly-ubiquitination is similar, we tested the effect of ubiquitin mutants on ubiquitination of Art2 by GID^{SR10}. A lysine-less ubiquitin was unable to support robust poly-ubiquitination of Art2 (Fig EV4A), suggesting that GID^{SR10} indeed catalyzes the formation of poly-ubiquitin chains. Interestingly, both an otherwise lysine-less ubiquitin containing only K48 or a ubiquitin containing a singly K48R point mutation supported poly-ubiquitination of Art2 (Fig EV4A), suggesting that GID^{SR10} is capable of forming a mixture of K48 and non-K48 ubiquitin chains. To further confirm the ubiquitination activity of GID^{SR10} toward Art2, we used a peptide substrate consisting of residues 2–29 of Art2, which includes an endogenously ubiquitinated lysine at position 26 (Swaney *et al*, 2013). In the presence of GID^{SR10}, we observed poly-ubiquitination of this peptide substrate, which was dependent on the N-terminal proline. GID^{SR4} also mediated low-level ubiquitination of the peptide substrate (Fig 5D), which suggests the potential to interact in the context of a fully-assembled E3. Taken together, our results indicate that Art2 is a substrate of GID^{SR10}.

A GID phenotype for amino acid uptake

Art2 is one of a suite of ART adaptors that guides the Nedd4 family E3 ubiquitin ligase Rsp5 to plasma membrane transporters, and directs their selective endocytosis (Lauwers *et al*, 2010; Babst, 2020). Intriguingly, Rsp5, the Rsp5-associated deubiquitinase Ubp2, and the α-arrestin Art3 also contain a proline at position 2, and therefore may parallel other GID E3 substrates and be processed by methionine aminopeptidase to exist in cells with an N-terminal proline. Thus, we tested if Gid10 and/or Gid4 bind the N-terminal sequences of Rsp5, Ubp2 or members of the α-arrestin family. However, our yeast two-hybrid assay revealed only the Gid10-Art2 interaction, further highlighting its specificity (Fig EV4B–E).

Compared with other ARTs, the functions of Art2 are relatively poorly characterized, in part because of redundancy with other more functionally dominant family members, and in part because its relatively large size and protein properties make biochemical

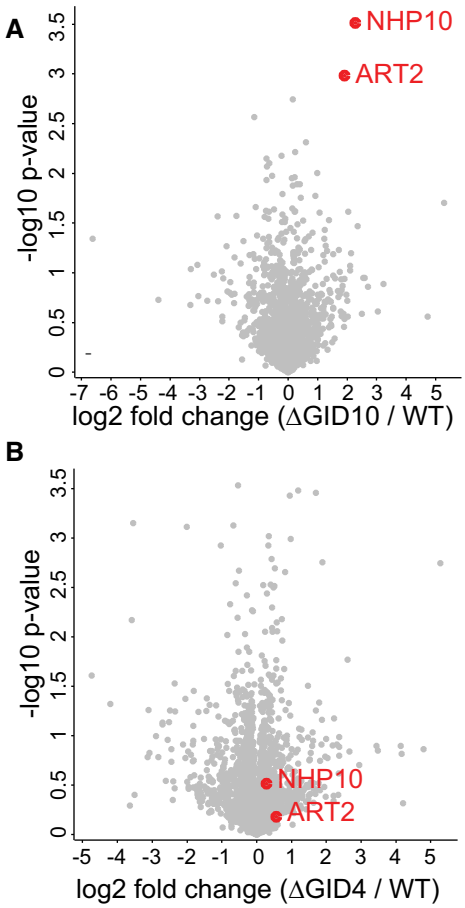

Figure 3. Art2 is upregulated in the absence of Gid10 during heat shock.

A Volcano plot of the (−log10) *P*-values versus the log2 protein abundance differences between Gid10 null yeast versus WT. Red dots indicate significantly different proteins, determined based on *P*-value < 0.01 and at least 4-fold change.

B Volcano plot of the (−log10) *P*-values versus the log2 protein abundance differences between Gid4 null yeast versus WT. Red dots indicate significantly different proteins in the comparison of Gid10 null yeast versus WT shown in A.

analyses challenging. Nonetheless, Art2 has been associated with endocytosis and vacuolar degradation of the lysine permease, Lyp1, during some environmental perturbations, including amino acid starvation, nitrogen starvation, and cycloheximide treatment (Lin *et al*, 2008; Ivashov *et al*, 2020). Thus, we tested if the GID complex plays a role in Lyp1 regulation by examining phenotypes on the toxic lysine analog, thialysine (S-Aminoethyl-l-cysteine), with the rationale that cells will be hypersensitive to thialysine when Lyp1 is stabilized at the plasma membrane. Importantly, both Art2 deletion and an Art2^{P2S} mutant also showed delayed growth on thialysine (Fig 6A), suggesting that the Art2 deletion effect can at least partly be attributed to regulation by the GID E3 ligase. Furthermore, individual deletions of all GID core subunits, with the exception of Gid7, which is dispensable for some substrates (Negoro *et al*, 2020; Kong *et al*, 2021; Sherpa *et al*, 2021), as well as a double deletion of *GID4* and *GID10* resulted in cellular toxicity during growth on thialysine, even in the absence of an additional stress condition (Fig 6B and C). The requirement for both SRs (Fig 6C) suggests that there may be some overlap in SR function *in vivo*, consistent with the low level of GID^{SR4} activity observed in the *in vitro* ubiquitination assay (Fig 4D). The similar phenotypes for all core subunits suggest a role in regulation of Lyp1 receptor localization or activity.

Thus, we used a GFP protection assay to determine whether the GID E3 ligase impacts Lyp1 import and degradation. This assay takes advantage of the fact that GFP is resistant to vacuolar degradation, but proteins fused to it typically are not. Thus, vacuolar degradation of GFP-tagged proteins can be monitored by Western blot, where undegraded protein will appear as a full-length-GFP band, and the appearance of a free GFP band reflects delivery of the GFP-tagged protein to the vacuole (Cheong & Klionsky, 2008). Surprisingly, performing this assay with Lyp1-GFP showed that Lyp1 import and degradation during heat shock remained unchanged in the GID mutant strains (Fig EV5A), despite the effect of these mutations on yeast growth on thialysine. In addition to Art2 regulation of Lyp1, another ART protein, Art1, has also been shown to regulate Lyp1 import and degradation in response to lysine excess, thialysine treatment, and heat stress (Lin *et al*, 2008; Zhao *et al*, 2013; Baile *et al*, 2019), suggesting that GID-dependent regulation of Art2 may not be the main mechanism to promote Lyp1 import during heat stress. Indeed, we observe that thialysine toxicity is increased and Lyp1 import and degradation is reduced in an *ART1* deletion, compared with wildtype, and a double deletion of *ART1* and *ART2* is further impaired (Fig EV5B and C). These data suggest that Art1 is the main regulator of Lyp1 during heat stress, but Art2 also contributes to this regulation. Notably, as observed for *ART1ART2* double deletion, in the absence of Art1, deletion of a core subunit or Gid10 resulted in increased toxicity during growth on thialysine (Fig 6D and E).

Deletion of the GID core subunits Gid2 or Gid5 results in impaired Lyp1 import and degradation in the ΔArt1 background (Fig EV5D). Interestingly, when compared with single deletions, deletion of both Art2 and a GID core subunit resulted in a slightly stronger phenotype on thialysine (Fig EV5E), and slightly greater impairment in Lyp1 import and degradation (Fig EV5F and G), raising the possibility that the GID E3 ligase plays both Art2-dependent and Art2-independent roles in plasma membrane nutrient transporter regulation. Taken together, these data indicate that GID^{SR10}, and to a lesser extent GID^{SR4}, modulate Art2 function to affect the flux of plasma membrane nutrient transporters; however, future experiments will be required to identify the exact mechanism.

Genetic interaction between the GID E3 ligase and an Art2-Rsp5 pathway

Art2 recruits Rsp5 to plasma membrane nutrient transporters and thereby promotes their endocytosis. Thus, to better understand the molecular mechanism although which the GID ligase regulates plasma membrane nutrient transporters, we probed the genetic interaction between the GID ligase, Art2 and Rsp5. Notably, ubiquitination of other Rsp5 adaptor proteins promotes their interaction with Rsp5 in a manner depending on Rsp5's ubiquitin-binding exosite (MacDonald *et al*, 2020). Thus, one intriguing possibility is that ubiquitinated Art2 may also employ this exosite in binding to Rsp5. Ubiquitin binding to such HECT E3 exosites has pleiotropic mechanistic roles, including allosterically activating ubiquitin transferase activity, contributing to processivity of the

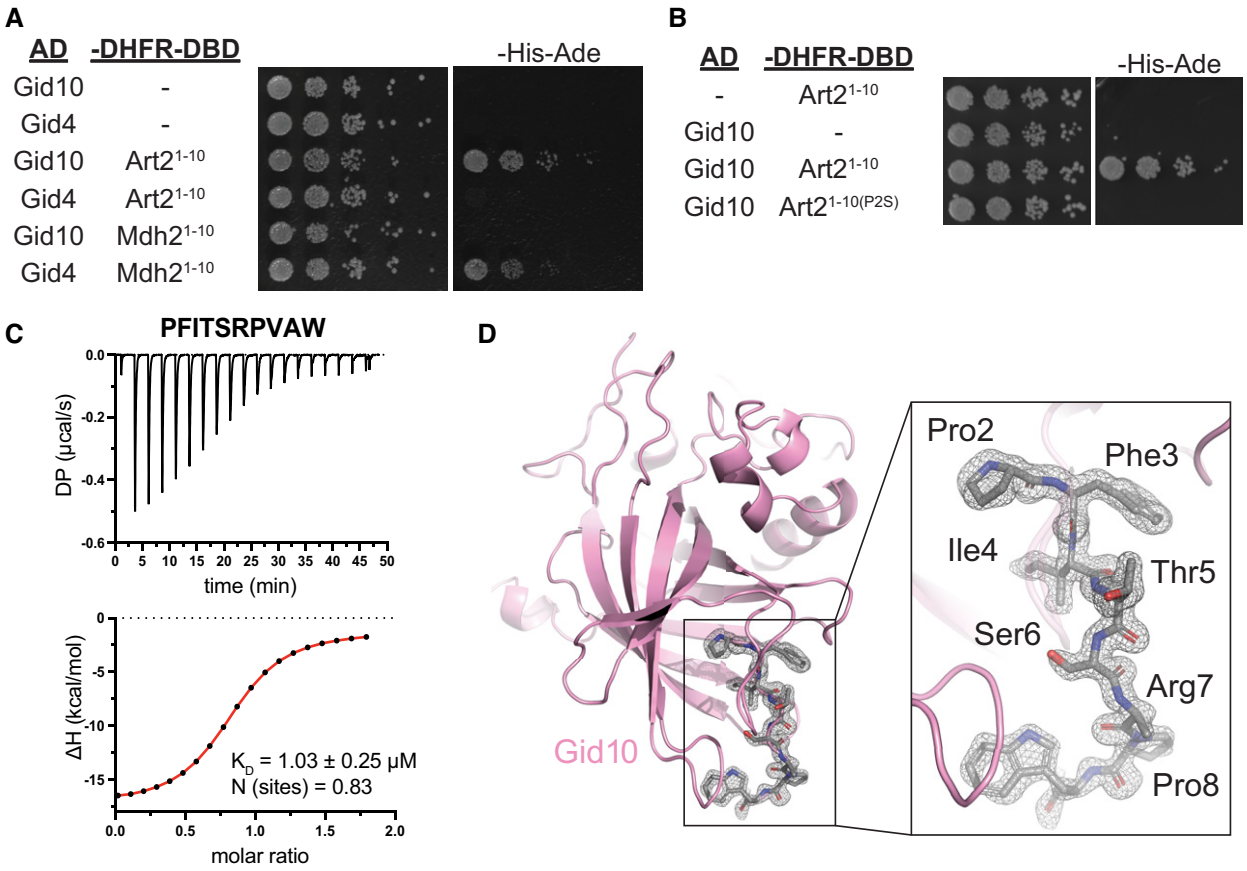

Figure 4. Art2 binds to Gid10 via its N-terminal proline.

A Yeast two-hybrid between SR-Gal4 activation domain (AD) and substrate degrons fused to DHFR-DNA binding domain (-DHFR-DBD). Growth on -His-Ade is indicative of an interaction between the two test proteins. Spots represent 1:5 serial dilutions.

B Yeast two-hybrid between Gid10-Gal4-AD and the $Art2^{WT}$ or $Art2^{P2S}$ degron fused to DHFR-DBD. Growth on -His-Ade is indicative of an interaction between the two test proteins. Spots represent 1:5 serial dilutions.

C Isothermal titration calorimetry (ITC) binding assay to quantify affinity (K_D) of $Art2^{2-9}$ degron for $Gid10^{57-292}$ substrate-binding domain. The raw ITC results (top) were integrated to calculate the amount of heat released (ΔH) during every injection of a peptide and plotted as a function of peptide:protein molar ratio (bottom). Fitting of the obtained data points to the binding model served to determine K_D and stoichiometry of the binding reaction (N).

D 1.3 Å-resolution crystal structure of $Gid10^{65-284}$ substrate-binding domain (pink cartoon) in complex with $Art2^{2-8}$ degron (gray sticks, C-terminal Trp was attached to accurately measure peptide concentration). The gray mesh represents electron density corresponding to the Art2 peptide.

poly-ubiquitination reaction, and recruiting ubiquitinated partner proteins including adaptor proteins. Nonetheless, an Rsp5 point mutant (F618A) that impairs ubiquitin binding is useful for probing genetic interactions (French *et al*, 2009; Kim *et al*, 2011; Maspero *et al*, 2011; Kathman *et al*, 2015; Zhang *et al*, 2016). While the $Rsp5^{F618A}$ mutation alone showed a strong growth defect on thialysine, the combination of a deletion of a GID core subunit and $Rsp5^{F618A}$ resulted in stronger toxicity on thialysine than either mutation alone (Fig 6F), suggesting that GID-dependent ubiquitination of Art2 is acting independently from the ubiquitin binding function of Rsp5. Next, we tested if GID-dependent Art2 ubiquitination might affect its ability to interact with Rsp5 though the canonical WW-PPx(Y/F) interaction motifs. While Rsp5 and Art2 contain multiple WW and PPx(Y/F) domains, respectively, the Rsp5-Art2 interaction is primarily mediated by the third WW domain of Rsp5 and the second PPx(Y/F) domain of Art2 (Ivashov *et al*, 2020). The combination of a core GID subunit deletion and either a mutation in the second Art2 PPx(Y/F) motif or the third WW Rsp5 domain did not result in stronger toxicity on thialysine than either mutation alone (Fig 6G and H), suggesting that the effect of the GID E3 ligase is dependent on the canonical WW-PPx (Y/F) interaction. Taken together, our data suggest that the GID E3 ligase ubiquitinates Art2 and thereby affects its ability to interact with Rsp5.

Discussion

Here, we demonstrate that the GID E3 ligase is a multifunctional metabolic regulator that incorporates different SRs in response to distinct stresses. We show that Gid10 is a bona fide substrate receptor by identifying Art2 as a protein that binds Gid10 through specific contacts directed by its N-terminal proline, and is ubiquitinated by GID^{SR10}. Furthermore, we identify for the first time a

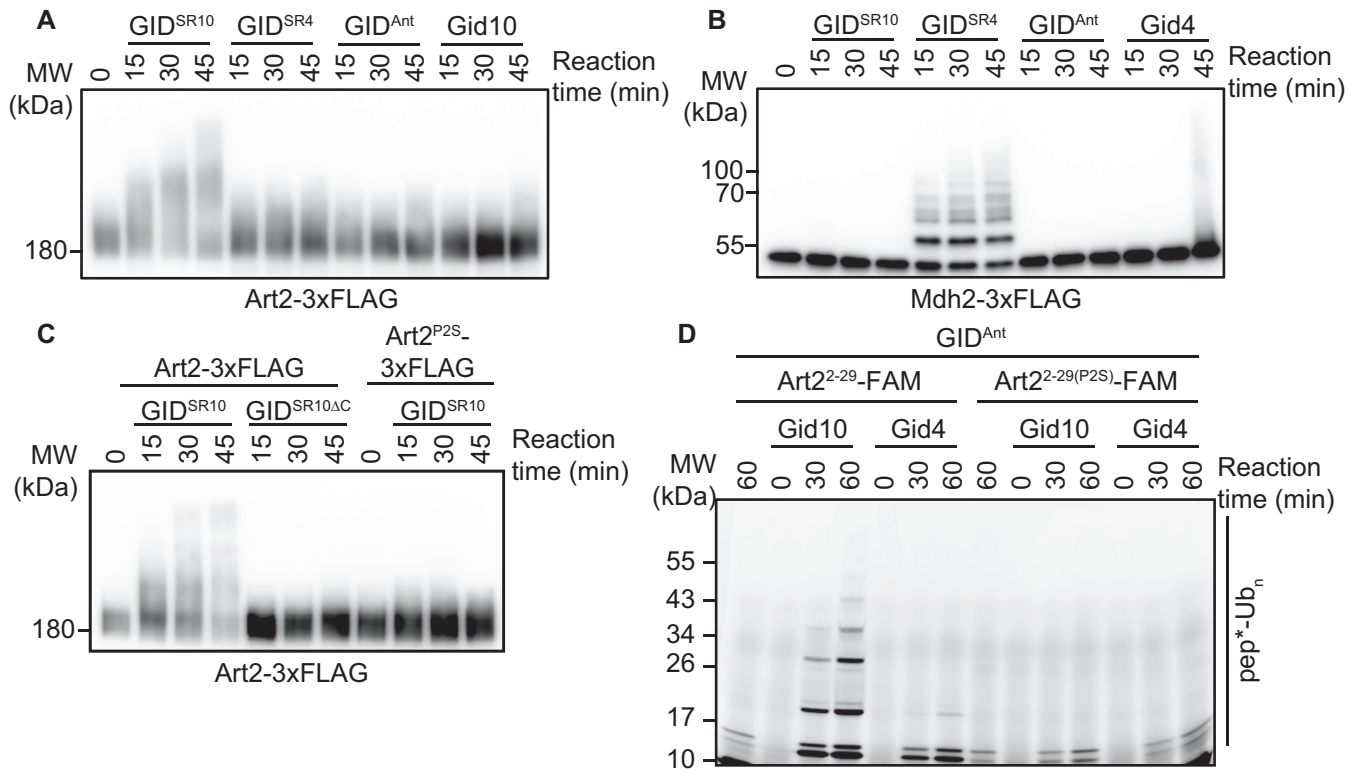

Figure 5. Gid^{SR10} ubiquitinates Art2.

A Art2-3xFLAG was immunocaptured from yeast cells grown in YPD and incubated with GID^{SR10}, GID^{SR4}, GID^{Ant}, or Gid10 for the indicated timepoints. Progress of the reaction was followed by αFLAG immunoblot.

B Mdh2-3xFLAG was immunocaptured from yeast cells following growth in YPE for 19 h and incubated with GID^{SR10}, GID^{SR4}, GID^{Ant}, or Gid4 for the indicated timepoints. Progress of the reaction was followed by αFLAG immunoblot.

C Art2-3xFLAG or Art2^{P2S}-3xFLAG was immunocaptured from yeast cells grown in YPD and incubated with GID^{SR10}, or GID$^{SR10\Delta C}$ for the indicated timepoints. Progress of the reaction was followed by αFLAG immunoblot.

D *In vitro* ubiquitination assay probing the ability of Gid10 and Gid4 to promote ubiquitination of Art2$^{2-29}$ N-terminus and its P2S mutant. Progress of the reaction was monitored by fluorescent scan of the gel visualizing the Art2 peptide with FAM appended to its C-terminus (pep*).

physiological phenotype for the yeast GID complex: increased sensitivity to thialysine, which is dependent on core GID subunits and both SRs.

Through ubiquitination of Art2, the GID E3 could affect the activity of another E3, Rsp5. Indeed, Art2 is a modulator of Rsp5, and we found that GID influences the import and degradation of the Rsp5 target Lyp1. This regulation depends on the interaction between the Art2 PPx(Y/F) domain and the Rsp5 WW domain, although the exact mechanism remains elusive. In addition, reversing the activity of Gid2 has been shown to disrupt growth on low-tryptophan media (MacDonald *et al*, 2017), implicating GID in the regulation of even more plasma membrane receptors. Both plasma membrane protein trafficking and Rsp5 interactions are intricately regulated by ubiquitin. Thus, Art2 ubiquitination could impact the ART-Rsp5 network in several ways. First, ubiquitination of Art2 by GID^{SR10} may lead to its deactivation, or promote its degradation. Indeed, our initial proteomics screen showed the levels of Art2 are modestly increased in a Gid10 deletion strain, which led to its discovery as a substrate. Notably, all previously identified GID E3 ligase substrates have been shown to undergo proteasomal degradation following ubiquitination. Although the deactivation of Art2 would impact its role as an Rsp5 adaptor, the inherent complexity, redundancy and interconnectedness of the ART-Rsp5 network raises the possibility that loss of Art2 might not exclusively result in loss of Rsp5 ubiquitination. Rather, relieved of interaction with Art2, Rsp5 could become more available for interactions with other arrestins, which could compensate for loss of Art2, or alternatively shift its preference to non-Art2-dependent targets. Second, Art2 ubiquitination could modulate its protein-protein interactions or activities. Ubiquitinated Art2 may have a different sub-cellular localization or affinity to Rsp5, as compared with unmodified Art2. Moreover, ubiquitination could impact multiple Art2 functions simultaneously. Ubiquitination of Art2 may also selectively affect its ability to interact with its plasma membrane targets, leading to a higher affinity for some targets, but a lower affinity for others. Future studies will be required to identify precisely how post-translational modifications modulate the ART-Rsp5 network, specific mechanisms impacted by GID E3-dependent ubiquitination of Art2, and the molecular details underlying the relationship between the GID E3 ligase and plasma membrane nutrient transporters.

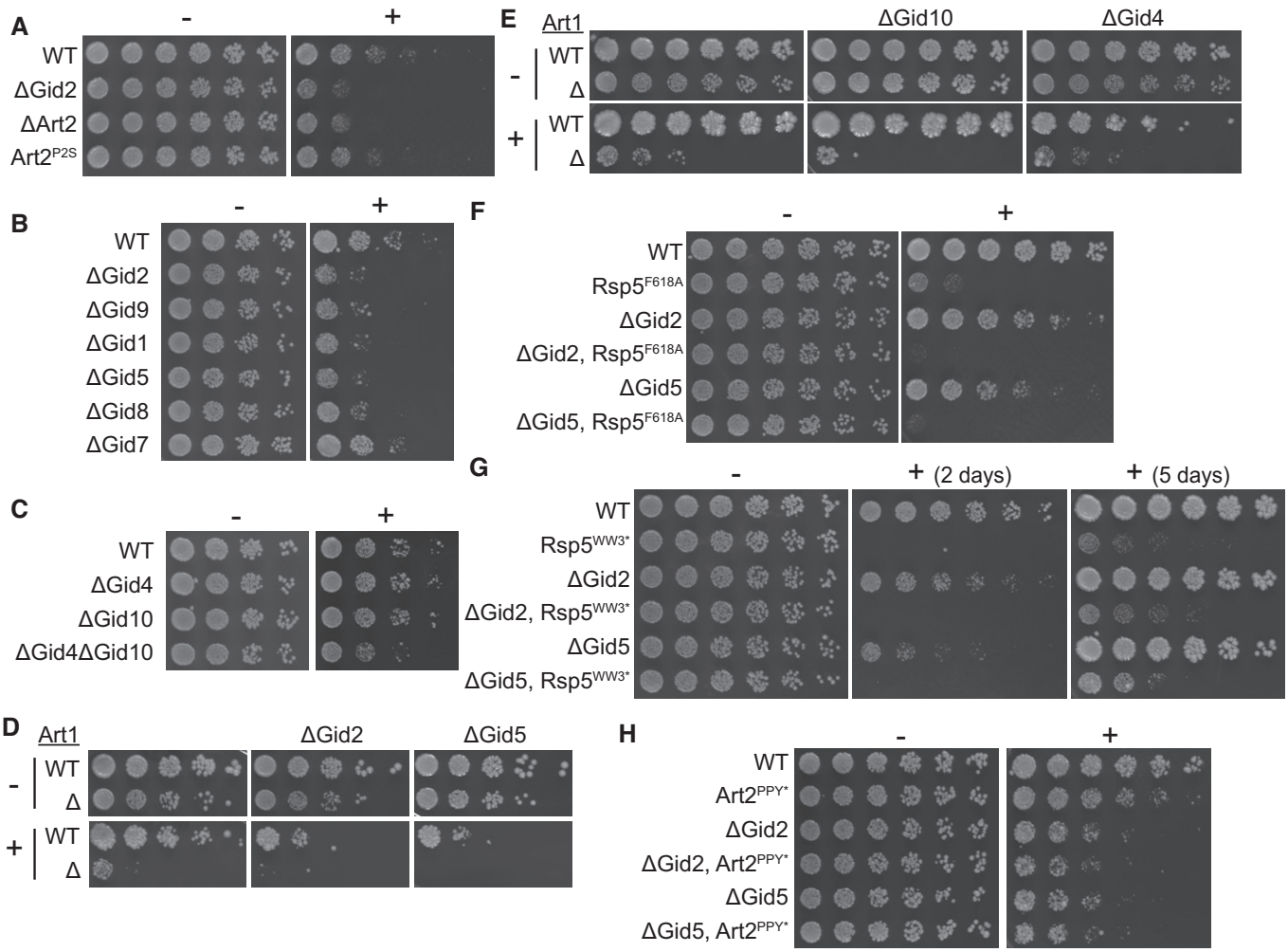

Figure 6. The GID E3 ligase affects flux of plasma membrane nutrient transporters.

A Growth assay of wildtype, ΔGid2, ΔArt2, and Art2^{P2S} yeast strains on SD-Lys (–) and SD-Lys containing 1.0 μg/ml thialysine (+). Spots represent 1:2.6 serial dilutions.

B Growth assay of wildtype yeast or yeast strains containing the indicated deletions on SD-Lys (–) and SD-Lys containing 1.5 μg/ml thialysine (+). Spots represent 1:5 serial dilutions.

C Growth assay of wildtype yeast or yeast strains containing the indicated deletions on SD-Lys (–) and SD-Lys containing 1.5 μg/ml thialysine (+). Spots represent 1:5 serial dilutions.

D Growth assay of wildtype and ΔArt1 strains containing *GID2* or *GID5* deletions on SD-Lys (–) and SD-Lys containing 1.0 μg/ml thialysine (+). Spots represent 1:5 serial dilutions.

E Growth assay of wildtype and ΔArt1 strains containing *GID10* or *GID4* deletions on SD-Lys (–) and SD-Lys containing 1.0 μg/ml thialysine (+). Spots represent 1:2.6 serial dilutions.

F Growth assay of wildtype and Rsp5^{F618A} strains containing *GID2* or *GID5* deletions on SD-Lys (–) and SD-Lys containing 0.75 μg/ml thialysine (+). Spots represent 1:2.6 serial dilutions.

G Growth assay of wildtype and Rsp5^{W415F,P418A} (Rsp5^{WW3*}) strains containing *GID2* or *GID5* deletions on SD-Lys (–) and SD-Lys containing 0.5 μg/ml thialysine (+). Spots represent 1:2.6 serial dilutions.

H Growth assay of wildtype and Art2^{P748A,P749A,Y750A} (Art2^{PPY*}) strains containing *GID2* or *GID5* deletions on SD-Lys (–) and SD-Lys containing 1.0 μg/ml thialysine (+). Spots represent 1:2.6 serial dilutions.

Interestingly, previous studies have also linked the GID E3 ligase to regulation of plasma membrane proteins. First, some GID complex subunits have been shown to play a role in the Vacuolar Import and Degradation (VID) pathway, which brings proteins to the vacuole for degradation following their endocytosis from the plasma membrane (Brown *et al*, 2010; Giardina *et al*, 2013). Second, it has been shown that the signals which lead to the degradation of Fbp1 and the hexose transporter Gal2 likely originate from the same biochemical pathway (Horak *et al*, 2002). Third, Gid11 was recently identified as an additional SR of the GID complex. The Gid11 protein also regulates metabolic enzymes involved in amino acid and nucleotide biosynthesis (Kong *et al*, 2021), and deletion of *GID11* leads to defects in plasma membrane electron transport (Herst *et al*, 2008), suggesting an additional role for Gid11 in regulation of plasma

membrane proteins. Importantly, expression of each SR is only induced during a distinct subset of environmental perturbations. Because each environmental change leads to vast, but distinct, remodeling of cellular metabolism, we propose that the GID E3 ligase may have evolved as a common node to regulate nutrient import across the plasma membrane and subsequent cellular synthesis of the necessary metabolites.

Although the GID E3 ligase has long been characterized as functioning during glucose-induced glycolysis, we show that the GID E3 ligase additionally regulates amino acid transporters, and also that there is a GID phenotype linked to amino acid metabolism, similar to effects observed when deleting ART proteins. What advantages might arise from a singular core E3 complex with distinct inputs from and outputs to multiple metabolic pathways? Because environmental changes are often abrupt, the activation of the complex through incorporation of a single protein allows yeast cells to respond rapidly. In addition, the transient expression of SRs, which we show depends on both GID complex activity and SR-GID^{Ant} binding, ensures that substrate selection by GID^{SR} is limited to a pulse following a switch in environmental conditions. Thus, the GID E3 ligase employs rapid "on" and "off" switches which allow it to rapidly and specifically respond to environmental perturbations.

We speculate that the GID E3 may be poised like other post-translational modifying enzymes that serve as metabolic nodes. For example, abundance or paucity of particular metabolites regulate kinase activities of mTOR, which like the GID E3 assembles into different complexes to regulate specific sets of biosynthetic and catabolic processes. Although the GID E3 is not essential in yeast under normal growth conditions, our work suggests there could be distinct requirements under particular environments. Moreover, the GID complex in higher eukaryotes, (termed CTLH—for C-Terminal to LisH) regulates important physiology and is essential for viability (Salemi *et al*, 2017; Lampert *et al*, 2018). Intriguingly, the CTLH complex serves as a regulator of autophagic flux and mTOR signaling, key pathways that integrate cellular responses to environmental changes (Liu *et al*, 2020). While more studies are needed to characterize additional GID regulatory targets, it is clear that the GID E3 ligase is implicated in diverse cellular pathways throughout eukaryotes and serves to enable rapid and robust cellular responses to environmental perturbations.

Materials and Methods

All plasmids and yeast strains used in this study are listed in Tables 1 and 2, respectively.

Yeast strains and growth conditions

All yeast strains were constructed using standard techniques (Knop *et al*, 1999; Storici & Resnick, 2003; Janke *et al*, 2004). Yeast were grown in YPD (1% yeast extract, 2% peptone, 2% glucose) or SD complete (0.67% yeast nitrogen base without amino acids, 2% glucose, containing 87.5 mg/l alanine, arginine, asparagine, aspartic acid, cysteine, glutamine, glutamic acid, glycine, leucine, lysine, methionine, myo-inositol, isoleucine, phenylalanine, proline, serine, threonine, tyrosine and valine, 43.7 mg/l histidine, tryptophan and uracil,

Table 1. Plasmids used in this study.

Plasmid	Description	Reference
pCSJ95	pRS313-$P_{TDH3(modified)}$-Fbp1-3xFLAG-CYC-$P_{TDH3(modified)}$-FLAG-DHFR-HA-CYC	Chen *et al* (2017)
pCSJ125	pRS313-$P_{TDH3(modified)}$-Mdh2-3xFLAG-CYC-$P_{TDH3(modified)}$-FLAG-DHFR-HA-CYC	Chen *et al* (2017)
pGADCg	Y2H expression vector. Contains the P_{ADH1} promoter, used to produce Gal4-AD-HA fusions.	Addgene (Cat#20161)
pGBKCg	Y2H expression vector. Contains the P_{ADH1} promoter, used to produce Gal4-DBD-Myc fusions.	Addgene (Cat#20162)
pCSJ182	pGADCg-NLS-Gid4-3xFLAG-Gal4-AD	Chen *et al* (2017)
pCSJ392	pGADCg-NLS-Gid10-3xFLAG-Gal4-AD	Melnykov *et al* (2019)
CRLP81	pGBKCg-Gid5-Gal4-DBD	This study
CRLP83	pGADCg-DHFR-Gal4-AD	This study
VBP43	pGBKCg-Rsp5$^{1-10}$-DHFR-Gal4-DBD	This study
VBP44	pGBKCg-Nhp10$^{1-10}$-DHFR-Gal4-DBD	This study
VBP45	pGBKCg-Art2$^{1-10}$-DHFR-Gal4-DBD	This study
VBP55	pGBKCg-Mdh2$^{1-10}$-DHFR-Gal4-DBD	This study
VBP57	pGBKCg-Fbp1$^{1-10}$-DHFR-Gal4-DBD	This study
VBP58	pGBKCg-DHFR-Gal4-DBD	This study
VBP60	pGBKCg-Art2$^{1-10(P2S)}$-DHFR-Gal4-DBD	This study
VBP69	pGBKCg-Art1$^{1-10}$-DHFR-Gal4-DBD	This study
VBP70	pGBKCg-Art3$^{1-10}$-DHFR-Gal4-DBD	This study
VBP71	pGBKCg-Art4$^{1-10}$-DHFR-Gal4-DBD	This study
VBP72	pGBKCg-Art5$^{1-10}$-DHFR-Gal4-DBD	This study
VBP73	pGBKCg-Art6$^{1-10}$-DHFR-Gal4-DBD	This study
VBP74	pGBKCg-Art7$^{1-10}$-DHFR-Gal4-DBD	This study
VBP75	pGBKCg-Art8$^{1-10}$-DHFR-Gal4-DBD	This study
VBP76	pGBKCg-Art9$^{1-10}$-DHFR-Gal4-DBD	This study
VBP77	pGBKCg-Art10$^{1-10}$-DHFR-Gal4-DBD	This study
VBP78	pGBKCg-Bul1$^{1-10}$-DHFR-Gal4-DBD	This study
VBP79	pGBKCg-Bul2$^{1-10}$-DHFR-Gal4-DBD	This study
VBP80	pGBKCg-Ubp2$^{1-10}$-DHFR-Gal4-DBD	This study
JCDS01	pLIB-Gid5	Qiao *et al* (2020)
JCDS02	pLIB-Gid5 W606A/Y613A/Q649A	Qiao *et al* (2020)
JCDS03	pBIG2-Gid1:Gid8-TEV-2xS:Gid5:Gid2:Gid9	Qiao *et al* (2020)
JCDS04	pBIG2-Gid1:Gid8-TEV-2xS:Gid2:Gid9	Qiao *et al* (2020)
JCDS05	pGEX-GST-TEV-Gid4 (117-362)	Qiao *et al* (2020)
JCDS06	pGEX-GST-TEV-Gid4 (117-358)	Qiao *et al* (2020)
JCDS07	pGEX-GST-TEV-Gid10 (57-292)	Qiao *et al* (2020)

Table 1 (continued)

Plasmid	Description	Reference
JCDS08	pGEX-GST-TEV-Gid10 (57-288)	Qiao *et al* (2020)
JCDS09	pGEX-GST-TEV-Gid10 (65-284)	This study
JCDS10	pRSF-Ubc8-6xHis	Qiao *et al* (2020)
JCDS11	PET3b-Ub	Qiao *et al* (2020)
JCDS12	pLIB-2xS-3c-Gid4	This study
JCDS13	pBIG2-Gid1:Gid8:Gid5:2xS-3c-Gid10:Gid2:Gid9	This study

22.5 mg/l adenine, and 8.7 mg/l para-aminobenzoic acid) media. Where plasmids are used, the appropriate amino acids were omitted from SD complete media. YPE and SE growth media indicate replacement of the glucose in YPD or SD complete, respectively, with 2% ethanol. For nutrient starvation, yeast cultures were grown to OD_{600} = 1.0 in SD complete, washed once with pre-warmed SD-AA (0.67% yeast nitrogen base without amino acids, 2% glucose, and 20 mg/l uracil) or SD-N (0.17% yeast nitrogen base without amino acids or ammonium sulfate, 2% glucose), resuspended in pre-warmed SD-AA or SD-N to an OD_{600} = 1, and grown for the indicated timepoints. Unless otherwise specified, yeast cultures were grown at 30°C.

Yeast growth assays

For yeast two-hybrid experiments, pGADCg- and pGBKCg-based plasmids containing the indicated protein fusions were transformed into the yeast strain Y2HGOLD (Takara Bio), and double transformants were selected by growth on SD media lacking leucine and tryptophan. Cells were then grown in SD media lacking leucine and tryptophan and supplemented with 0.1 mg/ml adenine to an OD_{600} of 1.0–2.0. A 240 µl dilution containing 0.096 ODs of cells was transferred to the first column of a sterile 96-well microtiter plate. Serial dilutions were made, at the dilutions specified, and yeast cells were spotted using a 48 Pin Multi-Blot Replicator (V&P Scientific VP480) on SD media lacking leucine and tryptophan, supplemented with 0.1 mg/ml adenine, and SD media lacking leucine, tryptophan, histidine and adenine (and, where indicated, supplemented with Aureobasidin A). Plates were grown at 30°C.

For growth assays on thialysine, yeast cells were grown in SD complete media to an OD of 1.0–2.0. Yeast cells were diluted as described above and spotted on SD lacking lysine, or SD lacking lysine supplemented with thialysine at the indicated concentrations.

Yeast cell lysis and western blotting

Protein degradation assays using the promoter reference technique were done as previously described (Oh *et al*, 2017). Cells were transformed with a plasmid expressing a test substrate and DHFR from identical promoters containing tetracycline-repressible RNA-binding elements. Yeast cells were grown in SD media lacking histidine to an OD_{600} of 1.0-1.5, pelleted by centrifugation at 3,000 rpm for 3 min, washed once with pre-warmed SE media lacking histidine, resuspended to an OD_{600} of 1.0 in pre-warmed SE media lacking histidine, and grown for 19 h. Cells were then pelleted by centrifugation at 3,000 rpm for 3 min, resuspended to an OD_{600} of

Table 2. Yeast strains used in this study.

Strain	Genotype	Reference
BY4741	*MATa his3Δ1 leu2Δ0 met15Δ0 ura3Δ0*	Euroscarf (Cat#Y00000)
CRLY12	*BY4741; gid4::KANMX*	Sherpa *et al* (2021)
CRLY13	*BY4741; gid5::KANMX*	This study
CRLY14	*BY4741; gid7::KANMX*	Sherpa *et al* (2021)
CRLY15	*BY4741; gid8:;KANMX*	This study
CRLY16	*BY4741; gid9:;KANMX*	This study
CRLY17	*BY4741; gid10::KANMX*	This study
CRLY30	*BY4741; gid2::KANMX*	This study
CRLY68	*BY4741; gid4::3xFLAG-GID4*	Qiao *et al* (2020)
CRLY74	*BY4741; gid10:3xFLAG-GID10*	Qiao *et al* (2020)
CRLY186	*BY4741; gid1::KANMX*	This study
CRLY296	*BY4741; gid10::NATNT2-P_{GPD}-GID10*	This study
CRLY298	*BY4741; gid4::KANMX gid10::NATNT2-pGPD-GID10*	This study
CRLY301	*BY4741; gid4::KANMX gid10::3xFLAG-GID10*	This study
CRLY314	*BY4741; gid10::3xFLAG-GID10 gid5::GID5-3xHA-KANMX*	This study
CRLY326	*BY4741; gid4::3xFLAG-GID4 gid5::Gid5-3xHA-KANMX*	This study
CRLY353	*BY4741; art2::ART2-3xFLAG-HPHNT1*	This study
CRLY365	*BY4741; gid10::3xFLAG-GID10 gid8::GID8-3xHA-KANMX gid4::NATNT2*	This study
CRLY382	*BY4741; lyp1::LYP1-GFP-HPHNT1*	This study
CRLY384	*BY4741; gid4::KANMX lyp1::LYP1-GFP-HPHNT1*	This study
CRLY386	*BY4741; gid10::KANMX lyp1::LYP1-GFP-HPHNT1*	This study
CRLY388	*BY4741; gid2::KANMX lyp1::LYP1-GFP-HPHNT1*	This study
CRLY407	*BY4741; art2::KANMX lyp1::LYP1-GFP-HPHNT1*	This study
CRLY431	*BY4741; art2::KANMX*	This study
CRLY434	*BY4741; art1::NATNT2*	This study
CRLY435	*BY4741; art1::NATNT2 can1::CAN1-GFP-HPHNT1*	This study
CRLY451	*BY4741; art1::NATNT2 lyp1::LYP1-GFP-HPHNT1*	This study
CRLY453	*BY4741; art2::KANMX art1::NATNT2 lyp1::LYP1-GFP-HPHNT1*	This study
CRLY458	*BY4741; art1::ART2(P2S)*	This study
CRLY460	*BY4741; art2::ART2(P748A,P749A,Y750A)*	This study
CRLY468	*BY4741; mdh2::MDH2-3xFLAG-HPHNT1*	This study
CRLY473	*BY4741; gid5::KANMX lyp1::LYP1-GFP-HPHNT1*	This study
CRLY487	*BY4741; art2::ART2(P2S)-3xFLAG-HPHNT1*	This study
CRLY490	*BY4741; art2::ART2(P748A,P749A,Y750A) gid2::KANMX*	This study

Table 2 (continued)

Strain	Genotype	Reference
CRLY492	*BY4741; art2::ART2(P748A,P749A,Y750A) gid5::KANMX*	This study
CRLY507	*BY4741; art2::NATNT2-P_{GPD}-ART2 art1::KANMX*	This study
CRLY517	*BY4741; art2::KANMX art1::NATNT2*	This study
CRLY520	*BY4741; gid5::KANMX art2::NATNT2*	This study
CRLY527	*BY4741; gid2::KANMX art2::NATNT2*	This study
CRLY569	*BY4741; gid4::3xFLAG-GID4 gid10::NATNT2-P_{GPD}-GID10*	This study
CRLY593	*BY4741; rsp5::RSP5(F618A) gid2::HPHNT1*	This study
CRLY595	*BY4741; rsp5::RSP5(F618A) gid5::HPHNT1*	This study
CRLY609	*BY4741; rsp5::RSP5(W415F, P418A)*	This study
CRLY626	*BY4741; rsp5::RSP5(W415F, P418A) gid2::HPHNT1*	This study
CRLY628	*BY4741; rsp5::RSP5(W415F, P418A) gid5::HPHNT1*	This study
LHY146	*BY4741; gid4::NATNT2 gid10::KANMX*	This study
VBY104	*BY4741; gid4::3xFLAG-GID4 gid5::GID5 (W606A,Y613A,Q649A)-3xHA-KANMX*	This study
VBY105	*BY4741; gid10::3xFLAG-GID10 gid5::GID5 (W606A,Y613A,Q649A)-3xHA-KANMX*	This study
VBY106	*BY4741; gid4::3xFLAG-GID4(F359A,F361A) gid5::GID5-3xHA-KANMX*	This study
VBY107	*BY4741; gid10::3xFLAG-GID10(Δ289-292) gid5::GID5-3xHA-KANMX*	This study
VBY109	*BY4741; gid4::GID4(F359A,F361A) gid10::3xFLAG-GID10*	This study
VBY110	*BY4741; gid4::3xFLAG-GID4 gid2::KANMX*	This study
VBY111	*BY4741; gid4::3xFLAG-GID4 gid10::KANMX*	This study
VBY119	*BY4741; gid2::KANMX art1::HPHNT1*	This study
VBY120	*BY4741; gid4::KANMX art1::HPHNT1*	This study
VBY121	*BY4741; gid5::KANMX art1::HPHNT1*	This study
VBY124	*BY4741; gid10::KANMX art1::HPHNT1*	This study
VBY130	*BY4741; gid4::KANMX art1::NATNT2 lyp1::LYP1-GFP-HPHNT1*	This study
VBY131	*BY4741; gid10::KANMX art1::NATNT2 lyp1::LYP1-GFP-HPHNT1*	This study
VBY132	*BY4741; gid2::KANMX art1::NATNT2 lyp1::LYP1-GFP-HPHNT1*	This study
VBY133	*BY4741; gid5::KANMX art1::NATNT2 lyp1::LYP1-GFP-HPHNT1*	This study
VBY153	*BY4741; rsp5::RSP5(F618A)*	This study
VBY155	*BY4741; gid4::KANMX gid10::NATNT2 art1::HISMX6 lyp1::LYP1-GFP-HPHNT1*	This study
VBY156	*BY4741; gid4::KANMX art1::NATNT2 can1::CAN1-GFP-HPHNT1*	This study
VBY157	*BY4741; gid10::KANMX art1::NATNT2 can1::CAN1-GFP-HPHNT1*	This study
VBY158	*BY4741; gid2::KANMX art1::NATNT2 can1::CAN1-GFP-HPHNT1*	This study
VBY159	*BY4741; gid5::KANMX art1::NATNT2 can1::CAN1-GFP-HPHNT1*	This study
Y2HGOLD	*MATa, trp1-901, leu2-3, 112, ura3-52, his3-200, gal4Δ, gal80Δ, LYS2::$GAL1_{UAS}$–$Gal1_{TATA}$–His3, $GAL2_{UAS}$–$Gal2_{TATA}$–Ade2 URA3::$MEL1_{UAS}$–$Mel1_{TATA}$A AUR1-C MEL1*	Takara Bio (Cat#630496)

1.0 in SD media lacking histidine and allowed to recover for the indicated timepoints. At each timepoint, 1 OD of yeast cells was pelleted, supernatant removed, flash-frozen in liquid nitrogen and stored at −80°C until lysis.

For lysis, yeast cells were resuspended in 0.8 ml 0.2 M NaOH, incubated 20 min on ice, and then pelleted by centrifugation at 11,200 *g* for 2 min. The supernatant was removed and the pellet was resuspended in 50 µl HU buffer and heated at 70°C for 10 min. Lysates were then pre-cleared by centrifugation at 11,200 *g* for 5 min and loaded onto a 12% SDS-PAGE gel. Samples were transferred to nitrocellulose membranes and visualized by Western blot using αFLAG (Sigma, F1804) and αHA (Sigma H6908) primary antibodies, and Dylight 633 goat anti-Mouse (Invitrogen 35512) and Dylight 488 goat anti-rabbit (Invitrogen 35552) secondary antibodies. Proteins were imaged on an Amersham typhoon scanner (GE Lifesciences), and bands were quantified with ImageStudio software (Licor).

For visualization of 3xFLAG-Gid4, 3xFLAG-Gid10, and Lyp1-GFP (where protein levels are not quantified), cells were grown under the indicated conditions, 5 ODs for 3xFLAG-Gid4 and 3xFLAG-Gid10 or 1.5 ODs for Lyp1-GFP of yeast cells were pelleted at each timepoint, and lysed as described above. Samples were run on a 12% SDS-PAGE gel, transferred to nitrocellulose membrane, and visualized by Western blot using αFLAG (Sigma, F1804) or αGFP (Roche 11814460001), and on a separate blot αPGK (Invitrogen 459250) primary antibodies, and goat anti-mouse peroxidase secondary antibody (Sigma A4416). Proteins were visualized on Amersham ImageQuant800 (GE Lifesciences). For visualization of 3xFLAG-Gid4 (where protein levels are quantified), 1.5 OD of yeast cells were pelleted at each timepoint and lysed as described above. Samples were run on a 12% SDS-PAGE gel, transferred to nitrocellulose membrane, and visualized by Western blotting using αFLAG (Sigma, F1804) and αPGK (Invitrogen 459250) primary antibodies on the same blot, and Dylight 633 goat anti-Mouse (Invitrogen 35512) secondary antibody.

Preparation of plasmids for recombinant protein expression

All constructs for bacterial protein expression were prepared by Gibson assembly method (Gibson *et al*, 2009). For generation of mutant versions of the genes, the QuickChange mutagenesis protocol was applied (Stratagene). All coding sequences used for protein expression were verified by DNA sequencing. To express the GID complex in insect cells from a single baculoviral expression vector, genes encoding GID subunits were combined by the biGBac assembly method (Weissmann *et al*, 2016).

Recombinant protein expression and purification

Both WT and mutant versions of the GID complex used for biochemical assays were expressed in Hi-5 insect cells transfected with recombinant baculovirus variants in EX-CELL 420 Serum-Free Medium. After 72 h at 27°C, the cultures were harvested and resuspended in a lysis buffer containing 50 mM HEPES pH 7.5, 200 mM NaCl, 5 mM DTT, 10 μg/ml leupeptin, 20 μg/ml aprotinin, 2 mM benzamidine, EDTA-free cOmplete protease inhibitor tablet (Roche, 1 tablet per 50 ml of buffer) and 1 mM PMSF. The complex was first affinity purified via a twin-Strep tag appended to Gid8 C-terminus. Further purification was performed by anion exchange chromatography and size exclusion chromatography (SEC) in the final buffer containing 25 mM HEPES pH 7.5, 200 mM NaCl and 1 mM DTT. For substrate receptor exchange experiment, the GID^{SR10} complex was affinity purified via a twin-Strep tag appended to Gid10 N-terminus. After pull-down, the tag was cleaved off by overnight 3c-protease cleavage. Similarly, Gid4 was expressed as an N-terminal twin-Strep tag fusion. The final purification was performed with SEC.

Aside from the GID complex and 2xS-Gid4, all recombinant proteins were expressed in *E. coli* BL21 (DE3) RIL. Cells transformed with an appropriate expression plasmid were grown in Terrific Broth (TB) medium at 37°C to an OD_{600} of 0.6 and cooled down to 18°C. Then, overnight expression of proteins was induced by addition of 0.4 mM IPTG. All versions of Gid4 and Gid10 were expressed as GST-TEV fusions. After harvesting, cell pellets were resuspended in the lysis buffer containing 50 mM HEPES pH 7.5, 200 mM NaCl, 5 mM DTT and 1 mM PMSF. GST-tagged proteins were purified from bacterial lysates by glutathione affinity chromatography, followed by overnight digestion at 4°C with tobacco etch virus (TEV) protease to cleave off the GST tag. Further purification was carried out with SEC in a buffer containing 25 mM HEPES pH 7.5, 150 mM NaCl and 1 mM DTT, 5 mM DTT or 0.5 mM TCEP for biochemical assays, crystallography and ITC binding test, respectively. At the end, a pass-back over glutathione affinity resin was performed to get rid of the remaining uncleaved GST-fusion protein and free GST. Ubc8 was expressed with a C-terminal 6xHis-tag. After harvesting, the cell pellet was resuspended in lysis buffer containing 50 mM HEPES pH 7.5, 200 mM NaCl, 5 mM β-mercaptoethanol, 10 mM imidazole and 1 mM PMSF. Ubc8-6xHis was purified by nickel affinity chromatography, followed by anion exchange and SEC. Untagged WT ubiquitin was purified via glacial acetic acid method (Kaiser *et al*, 2011), followed by gravity S column ion exchange chromatography and size exclusion chromatography.

Immunoprecipitation and ubiquitination assay

For Art2 ICs, yeast cells were grown in YPD at 30°C to an OD_{600} of 1.0–2.0. For Mdh2 ICs, yeast cells were grown in YPD to an OD_{600} of 1.0–1.5, pelleted by centrifugation at 3,000 rpm for 3 min, washed once with pre-warmed YPE, resuspended to an OD_{600} of 1.0 in fresh, pre-warmed YPE, and grown at 30°C for 19 h. 100 ODs of cells were pelleted by centrifugation at 3,000 rpm for 3 min, washed with dH_20, resuspended in 1 ml lysis buffer (50 mM Tris-HCL, pH 7.5, 150 mM NaCl, 2 mM EDTA, 50 mM NaF, 0.1% SDS, 1% NP-40, 0.5% Na-deoxycholate, 20 mM NEM, 1% glycerol, and cOmplete EDTA-free protease inhibitor tablets (Roche, 1 tablet per 10 ml buffer)), and transferred to a 2 ml tube containing lysing matrix C (MP Biomedicals). Cells were lysed by three rounds of 20 s in a Fast-Prep24 instrument (MP Biomedicals), resting on ice for 5 min in between each round. Lysates were then pre-cleared by centrifugation at 4,000 *g* for 10 min. The supernatant was added to 50 μl pre-washed anti-DYKDDDDK magnetic agarose beads (ThermoFischer A36797) and nutated at 4°C for 2 h. Beads were then separated on a magnetic rack, and supernatant was discarded. Beads were washed twice with wash buffer 1 (50 mM Tris-HCL, pH 7.5, 150 mM NaCl, 2 mM EDTA, 50 mM NaF, 0.1% SDS, 1%NP-40, 0.5% Na-deoxycholate, 20 mM NEM, 1% glycerol), twice with wash buffer 2 (25 mM HEPES, pH 7.5, 100 mM NaCl), and resuspended in 100 μl of wash buffer 2. For each ubiquitination reaction, 25 μl of this suspension were pelleted on a magnetic rack, and supernatant removed. Ubiquitination reaction mix (1 μM E2 Ubc8-6xHis, 0.5 μM GID^{Ant}, 30 μM Ubiquitin, 0.5 μM substrate receptor (none, $Gid10^{57–292}$, $Gid10^{57–288}$, or $Gid4^{117–362}$, as indicated), 25 mM HEPES, pH 7.5, 100 mM NaCl, 2.5 mM $MgCl_2$, and 1 mM ATP) was added to the beads. The reaction was started by the addition of 0.2 μM E1 Uba1 and incubated at room temperature for the indicated timepoints. Beads were then pelleted on a magnetic rack, washed with wash buffer 1, resuspended in 30 μl 2× sample buffer, and heated at 95°C for 5 min to elute the protein. For Art2-3xFLAG blots, the eluate was loaded on 4–12% SDS-PAGE gels, run at 200 V for 80 min, and transferred to PVDF membrane at 100 V for 90 min. For Mdh2-3xFLAG blots, eluate was loaded on a 12% SDS-PAGE gel, run at 200 V for 50 min, and transferred to nitrocellulose membrane at 100 V for 60 min. Samples were then visualized by immunoblotting with anti-FLAG (Sigma F1804) primary antibody and goat anti-mouse peroxidase secondary antibody (Sigma A4416), and imaged on an Amersham ImageQuant800 (GE Lifesciences).

In vitro binding assay

To test if the GID complex binds Gid10 in a manner similar to Gid4, WT and mutant versions (Gid5 W606A/Y613A/Q649A) of GID^{Ant} were mixed with 2-fold molar excess of $Gid10^{57–292}$, $Gid10^{57–288}$, $Gid4^{117–358}$ and $Gid4^{117–362}$. After incubating the proteins for 30 min on ice, 20 μl of Strep-Tactin resin was added to the mixture and further incubated for 30 min. After thorough wash of the resin, proteins were eluted and analyzed with SDS-PAGE.

In vitro competition binding assay

To test the swappable nature of GID substrate receptors, we competed binding of Gid10 to the GID^{SR10} complex with increasing concentrations of 2xS-Gid4. Briefly, 10 μM of untagged GID^{SR10} was mixed with strep-tactin either alone or after its 30-min incubation with 2xS-Gid4 (equimolar or added at 2- and 4-fold molar excess). After 30-min incubation, the resin was thoroughly washed with the wash buffer (25 mM HEPES pH 7.5, 150 mM NaCl and 5 mM DTT) and proteins were eluted. Substrate receptor exchange was assessed by inspecting the presence of the GID^{SR4} complex and absence of Gid10 in the strep pull-down fractions visualized by Coomassie-stained SDS-PAGE.

Isothermal titration calorimetry (ITC)

The ITC measurements were carried out with MicroCal PEAQ-ITC instrument (Malvern Panalytical) at 25°C. The Art2 degron peptide

was dissolved in the Gid10 SEC buffer containing 25 mM HEPES pH 7.5, 150 mM NaCl and 0.5 mM TCEP and their concentration was measured by absorbance at 280 nm. Binding experiments were carried out by titrating 450 μM peptide PFITSRPVAW to $Gid10^{57–292}$ at 42 μM. Peptide was added to Gid10 by nineteen 2 μl injections, with 4 s injection time and 150 s equilibration between the injections. The reference power was set to 10 μcal/s. Raw ITC data were analyzed using one site binding mode in MicroCal ITC analysis software (Malvern Panalytical) to determine K_D and stoichiometry of the binding reaction. All plots were prepared in GraphPad Prism.

In vitro ubiquitylation assay

To verify whether Art2 N-terminus can be ubiquitinated by GID^{SR10}, we performed an *in vitro* activity assay with $Art2^{2–29}$ WT and P2S mutant peptides, with fluorescein appended to their C-termini. Ubiquitination reaction was performed in a multi-turnover format in a buffer containing 25 mM HEPES pH 7.5, 150 mM NaCl, 5 mM ATP and 10 mM $MgCl_2$. To start the reaction, 0.2 μM E1 Uba1, 1 μM E2 Ubc8-6xHis, 0.5 μM E3 GID^{Ant}, 20 μM Ub, 0 or 1 μM $Gid4^{117–362}$ or $Gid10^{57–292}$ and 1 μM peptide substrate were mixed and incubated at room temperature. At indicated timepoints, an aliquot of the reaction mix was mixed with SDS-PAGE loading buffer. The outcome of the activity assay was visualized with a fluorescent scan of an SDS-PAGE gel with Typhoon imager (GE Healthcare).

Gid10 crystallization, data collection and structure determination

Crystallization trials were carried out in the MPIB crystallography facility. Before setting up crystallization trays, $Gid10^{65–284}$ was concentrated and mixed with PFITSRPW peptide to obtain final concentration of protein and peptide of 262 and 760 μM, respectively (~3-fold molar excess of the peptide). The crystal that gave rise to the final structure was grown at room temperature in the buffer containing 18.5% PEG3350, 0.1 M Bis-Tris propane pH 6.0 and 0.2 M potassium chloride by vapor diffusion in a sitting-drop format. Before data collection, crystals were cryoprotected in 20% ethylene glycol and flash-frozen in liquid nitrogen.

Diffraction data set was recorded at X10SA beam line, Swiss Light Source (SLS) in Villingen, Switzerland. Data were recorded at 0.5-degree rotation intervals using Dectris Eiger II 16 M detector. Data were indexed, integrated, and scaled using XDS package to a resolution limit of 1.3 Å. Phasing was performed through molecular replacement using a structure of yeast Gid4 (extracted from PDB: 7NS3) with PHASER integrated into the PHENIX software suite (Adams *et al*, 2010; DiMaio *et al*, 2013; Afonine *et al*, 2018). Model building was done using Coot (Emsley & Cowtan, 2004; Emsley *et al*, 2010), whereas refinement was carried out with phenix.refine. Details of X-ray diffraction data collection and refinement statistics are listed in Table EV1.

Proteomics sample preparation

Samples were prepared and analyzed as previously described (Karayel *et al*, 2020). Briefly, sodium deoxycholate (SDC) lysis buffer (1% SDC and 100 mM Tris, pH 8.5) were added to the frozen cell pellets. Lysates were immediately boiled for 5 min at 95°C and homogenized with sonication. Protein concentrations were estimated by tryptophan assay. Equal protein amounts were reduced and alkylated using CAA and TCEP, final concentrations of 40 and 10 mM, respectively, for 5 min at 45°C. Samples were digested overnight at 37°C using trypsin (1:100 wt/wt; Sigma-Aldrich) and LysC (1/100 wt/wt; Wako). Next, peptides were desalted using SDB-RPS StageTips (Empore). Samples were first diluted with 1% trifluoroacetic acid (TFA) in isopropanol to a final volume of 200 μl and loaded onto StageTips and subsequently washed with 200 μl of 1% TFA in isopropanol twice and 200 μl of 0.2% TFA/2% ACN (acetonitrile). Peptides were eluted with 80 μl of 1.25% Ammonium hydroxide (NH4OH)/80% ACN, dried using a SpeedVac centrifuge (Concentrator Plus; Eppendorf) and resuspended in buffer A* (0.2% TFA/2% ACN) prior to LC-MS/MS analysis. Peptide concentrations were measured optically at 280 nm (Nanodrop 2000; Thermo Scientific) and subsequently equalized using buffer A*. Three hundred nanograms of peptide was subjected to LC-MS/MS analysis.

LC-MS/MS measurements

DIA is a discovery-oriented acquisition method in which the quadrupole cycles through large *m/z* windows across the entire mass range to generate comprehensive fragment ion maps, covering nearly all detected precursors, and increasing the reproducibility, quantitative accuracy, and depth of proteome analysis in single runs compared with the conventional data-dependent acquisition (DDA) method, which takes only a selection of peptide signals forward for fragmentation.

Samples in panels 3A-B and EV2A were loaded onto a 20-cm reversed-phase column (75-μm inner diameter, packed in-house with ReproSil-Pur C18-AQ, 1.9 μm resin [Dr. Maisch GmbH]). The column temperature was maintained at 60°C using a homemade column oven. An EASY-nLC1200 system (Thermo Fisher Scientific), coupled with the mass spectrometer (Q Exactive HF-X, Thermo Fisher Scientific) via a nano-electrospray source, was employed for nano-flow liquid chromatography. A binary buffer system, consisting of buffer A (0.1% formic acid [FA]) and buffer B (0.1% FA and 80% ACN), was used for peptide separation, at a flow rate of 450 nl/min. We used a gradient starting at 5% buffer B, increased to 35% in 18.5 min, 95% in a minute, and stayed at 95% for 3.5 min. The mass spectrometer was operated in data independent acquisition mode (DIA). Full MS resolution was set to 120,000 with a full scan range of 300 to 1,650 *m/z*, a maximum fill time of 60 ms, and an AGC target of 3e6. One full scan was followed by 12 windows with a resolution of 30,000 in profile mode. Precursor ions were fragmented by stepped HCD (NCE 25.5, 27, and 30%).

Samples in panels 2C and EV2B were processed similarly except that peptide separation was at a flow rate of 300 nl/min and an EASY-nLC1200 system (Thermo Fisher Scientific) system was coupled with the mass spectrometer Orbitrap Exploris 480 (Thermo Fisher Scientific) via a nano-electrospray source. We used a gradient starting at 5% buffer B, increased to 30% in 45 min, 65% in 5 min, 95% in 5 min and stayed at 95% for 5 min. The mass spectrometer was operated in data independent acquisition mode (DIA). Full MS resolution was set to 120,000 with a full scan range of 300 to 1,650 *m/z*, a maximum fill time of 20 ms, and an AGC target of 3e6. One full scan was followed by 32 windows with a resolution of 30,000 in profile mode. Precursor ions were fragmented at NCE of 28%.

Data processing and bioinformatics analysis

The DIA files in panels 3A and B, and EV2A were analyzed using the proteome library previously generated (Karayel *et al*, 2020) with default settings and enabled cross-run normalization using Spectronaut version 13 (Biognosys AG). The files in panels 2C and EV2B were processed in Spectronaut version 15 (Biognosys AG). In both searches, we used the UniProt *S. cerevisiae* reference proteome of canonical and isoform sequences with 6,077 entries for final protein identification and quantification. We set carbamidomethylation as fixed modification and acetylation of the protein N-terminus and oxidation of methionine as variable modifications. Trypsin/P proteolytic cleavage rule was used with a maximum of two missed cleavages permitted and a peptide length of 7–52 amino acids. A protein and precursor FDR of 1% were used for filtering and subsequent reporting in samples (q-value mode with no imputation). The Perseus software package versions 1.6.0.7 and 1.6.0.9 (Tyanova *et al*, 2016) and GraphPad Prism version 7.03 were used for the data analysis. Protein intensities were log2-transformed, and the data sets were filtered to make sure that identified proteins showed expression or intensity in all biological triplicates of at least one condition and the missing values were subsequently replaced by random numbers that were drawn from a normal distribution (width = 0.3 and downshift = 1.8) in Perseus. To determine significantly different proteins, two sample t-test was applied, assuming that variance within the groups of replicates was equal. Data represent means ± SD ($n = 3$) and quantification was done by one-way ANOVA with Tukey's multiple comparisons test. $*P < 0.05$, $**P < 0.01$, $***P < 0.005$, $****P < 0.001$ to the corresponding legends and In panel 2C and EV2A, quantification was based on one-way ANOVA (unpaired), which is followed by Tukey's multiple comparison test to compare every mean with every other mean. The corrected P-values were shown in the panels.

Data availability

The structure of Gid10 bound to Art2 Pro/N-degron is available in RCSB under the accession code (PDB ID): 7QQY (http://www.rcsb.org/pdb/explore/explore.do?structureId=7QQY). The MS proteomics data have been deposited to the ProteomeXchange Consortium via the PRIDE database with the dataset identifier PXD030902 (https://www.ebi.ac.uk/pride/archive/projects/PXD030902).

Expanded View for this article is available online.

Acknowledgements

We thank R. Prabu und J. Basquin for assistance with crystallography; A. Varshavsky for providing PRT and Y2H plasmids; I. Paron for technical assistance; the Paul Scherrer Institut (Villigen, Switzerland) for provision of synchrotron radiation beamtime at beamline X10SA of the SLS; A. C. Michaelis, L. A. Hehl, F. Wilfling, S. von Gronau, M. Duennebacke, M. Lee, and all members of the Departments of Molecular Machines and Signaling and Proteomics and Signal Transduction for their advice and support. This study was supported by the Max Planck Gesellschaft, the European Research Council (ERC) under the European Union's Horizon 2020 research and innovation programme (grant agreement No 789016-NEDD8Activate), and the Gottfried Wilhelm Leibniz Prize from the Deutsche Forschungsgemeinschaft (DFG) (grant SCHU 3196/1-1). Open Access funding enabled and organized by Projekt DEAL.

Author contributions

Christine R Langlois: Conceptualization; Data curation; Formal analysis; Supervision; Investigation; Methodology; Writing—original draft; Writing—review & editing. **Viola Beier:** Investigation; Methodology; Writing—review & editing. **Ozge Karayel:** Investigation; Methodology; Writing—review & editing. **Jakub Chrustowicz:** Investigation; Methodology; Writing—review & editing. **Dawafuti Sherpa:** Investigation; Methodology; Writing—review & editing. **Matthias Mann:** Supervision; Funding acquisition; Writing—review & editing. **Brenda A Schulman:** Conceptualization; Supervision; Funding acquisition; Writing—review & editing.

In addition to the CRediT author contributions listed above, the contributions in detail are:

Conceptualization: CRL and BAS; Methodology and Investigation: CRL, VB, OK, DS, and JC; Writing—Original Draft: CRL; Writing—Review & Editing: CRL, VB, OK, DS, JC, and BAS; Supervision: CRL, MM, and BAS; Funding Acquisition: MM and BAS.

Disclosure and competing interests statement

The authors declare that they have no conflict of interest.

References

Adams PD, Afonine PV, Bunkóczi G, Chen VB, Davis IW, Echols N, Headd JJ, Hung L-W, Kapral GJ, Grosse-Kunstleve RW *et al* (2010) PHENIX: a comprehensive Python-based system for macromolecular structure solution. *Acta Crystallogr D Biol Crystallogr* 66: 213 – 221

Afonine PV, Poon BK, Read RJ, Sobolev OV, Terwilliger TC, Urzhumtsev A, Adams PD (2018) Real-space refinement in PHENIX for cryo-EM and crystallography. *Acta Crystallogr D Struct Biol* 74: 531 – 544

Babst M (2020) Regulation of nutrient transporters by metabolic and environmental stresses. *Curr Opin Cell Biol* 65: 35 – 41

Baile MG, Guiney EL, Sanford EJ, MacGurn JA, Smolka MB, Emr SD (2019) Activity of a ubiquitin ligase adaptor is regulated by disordered insertions in its arrestin domain. *Mol Biol Cell* 30: 3057 – 3072

Barnett JA, Entian K-D (2005) A history of research on yeasts 9: regulation of sugar metabolism. *Yeast* 22: 835 – 894

Becuwe M, Herrador A, Haguenauer-Tsapis R, Vincent O, Léon S (2012) Ubiquitin-mediated regulation of endocytosis by proteins of the arrestin family. *Biochem Res Int* 2012: 1 – 12

Brown CR, Dunton D, Chiang H-L (2010) The vacuole import and degradation pathway utilizes early steps of endocytosis and actin polymerization to deliver cargo proteins to the vacuole for degradation. *J Biol Chem* 285: 1516 – 1528

Cappadocia L, Lima CD (2018) Ubiquitin-like protein conjugation: structures, chemistry, and mechanism. *Chem Rev* 118: 889 – 918

Chen S-J, Wu X, Wadas B, Oh J-H, Varshavsky A (2017) An N-end rule pathway that recognizes proline and destroys gluconeogenic enzymes. *Science* 355: eaal3655–68

Cheong H, Klionsky DJ (2008) Biochemical methods to monitor autophagy-related processes in yeast. *Methods Enzymol* 451: 1 – 26

Deshaies RJ, Joazeiro CAP (2009) RING domain E3 ubiquitin ligases. *Annu Rev Biochem* 78: 399 – 434

DiMaio F, Echols N, Headd JJ, Terwilliger TC, Adams PD, Baker D (2013) Improved low-resolution crystallographic refinement with Phenix and Rosetta. *Nat Methods* 10: 1102 – 1104

Dong C, Chen S-J, Melnykov A, Weirich S, Sun K, Jeltsch A, Varshavsky A, Min J (2020) Recognition of nonproline N-terminal residues by the Pro/N-degron pathway. *Proc Natl Acad Sci USA* 117: 14158 – 14167

Dong C, Zhang H, Li L, Tempel W, Loppnau P, Min J (2018) Molecular basis of GID4-mediated recognition of degrons for the Pro/N-end rule pathway. *Nat Chem Biol* 14: 466 – 473

Dupré S, Urban-Grimal D, Haguenauer-Tsapis R (2004) Ubiquitin and endocytic internalization in yeast and animal cells. *Biochim Biophys Acta* 1695: 89 – 111

Emsley P, Cowtan K (2004) Coot: model-building tools for molecular graphics. *Acta Crystallogr D Biol Crystallogr* 60: 2126 – 2132

Emsley P, Lohkamp B, Scott WG, Cowtan K (2010) Features and development of coot. *Acta Crystallogr D Biol Crystallogr* 66: 486 – 501

Foot NJ, Dalton HE, Shearwin-Whyatt LM, Dorstyn L, Tan S-S, Yang B, Kumar S (2008) Regulation of the divalent metal ion transporter DMT1 and iron homeostasis by a ubiquitin-dependent mechanism involving Ndfips and WWP2. *Blood* 112: 4268 – 4275

French ME, Kretzmann BR, Hicke L (2009) Regulation of the RSP5 ubiquitin ligase by an intrinsic ubiquitin-binding site. *J Biol Chem* 284: 12071 – 12079

Gancedo JM (1998) Yeast carbon catabolite repression. *Microbiol Mol Biol Rev* 62: 334 – 361

Gasch AP, Spellman PT, Kao CM, Carmel-Harel O, Eisen MB, Storz G, Botstein D, Brown PO (2000) Genomic expression programs in the response of yeast cells to environmental changes. *Mol Biol Cell* 11: 4241 – 4257

Giardina BJ, Dunton D, Chiang H-L (2013) Vid28 protein is required for the association of vacuole import and degradation (Vid) vesicles with actin patches and the retention of Vid vesicle proteins in the intracellular fraction. *J Biol Chem* 288: 11636 – 11648

Gibson DG, Young L, Chuang R-Y, Venter JC, Hutchison CA, Smith HO (2009) Enzymatic assembly of DNA molecules up to several hundred kilobases. *Nat Methods* 6: 343 – 345

Hämmerle M, Bauer J, Rose M, Szallies A, Thumm M, Düsterhus S, Mecke D, Entian KD, Wolf DH (1998) Proteins of newly isolated mutants and the amino-terminal proline are essential for ubiquitin-proteasome-catalyzed catabolite degradation of fructose-1,6-bisphosphatase of *Saccharomyces cerevisiae*. *J Biol Chem* 273: 25000 – 25005

Herst PM, Perrone GG, Dawes IW, Bircham PW, Berridge MV (2008) Plasma membrane electron transport in *Saccharomyces cerevisiae* depends on the presence of mitochondrial respiratory subunits. *FEMS Yeast Res* 8: 897 – 905

Hettema EH, Valdez-Taubas J, Pelham HRB (2004) Bsd2 binds the ubiquitin ligase Rsp5 and mediates the ubiquitination of transmembrane proteins. *EMBO J* 23: 1279 – 1288

Horak J, Regelmann J, Wolf DH (2002) Two distinct proteolytic systems responsible for glucose-induced degradation of fructose-1,6-bisphosphatase and the Gal2p transporter in the yeast *Saccharomyces cerevisiae* share the same protein components of the glucose signaling pathway. *J Biol Chem* 277: 8248 – 8254

Hovsepian J, Defenouillère Q, Albanèse V, Váchová L, Garcia C, Palková Z, Léon S (2017) Multilevel regulation of an α-arrestin by glucose depletion controls hexose transporter endocytosis. *J Cell Biol* 216: 1811 – 1831

Huibregtse JM, Scheffner M, Howley PM (1993) Localization of the E6-AP regions that direct human papillomavirus E6 binding, association with p53, and ubiquitination of associated proteins. *Mol Cell Biol* 13: 4918 – 4927

Ivashov V, Zimmer J, Schwabl S, Kahlhofer J, Weys S, Gstir R, Jakschitz T, Kremser L, Bonn GK, Lindner H *et al* (2020) Complementary α-arrestin-ubiquitin ligase complexes control nutrient transporter endocytosis in response to amino acids. *Elife* 9: 1389

Janke C, Magiera MM, Rathfelder N, Taxis C, Reber S, Maekawa H, Moreno-Borchart A, Doenges G, Schwob E, Schiebel E *et al* (2004) A versatile toolbox for PCR-based tagging of yeast genes: new fluorescent proteins, more markers and promoter substitution cassettes. *Yeast* 21: 947 – 962

Kahlhofer J, Léon S, Teis D, Schmidt O (2020) The α-arrestin family of ubiquitin ligase adaptors links metabolism with selective endocytosis. *Biol Cell* 113: 183 – 219

Kaiser SE, Riley BE, Shaler TA, Trevino RS, Becker CH, Schulman H, Kopito RR (2011) Protein standard absolute quantification (PSAQ) method for the measurement of cellular ubiquitin pools. *Nat Methods* 8: 691 – 696

Karayel O, Michaelis AC, Mann M, Schulman BA, Langlois CR (2020) DIA-based systems biology approach unveils E3 ubiquitin ligase-dependent responses to a metabolic shift. *Proc Natl Acad Sci USA* 117: 32806 – 32815

Kathman SG, Span I, Smith AT, Xu Z, Zhan J, Rosenzweig AC, Statsyuk AV (2015) A small molecule that switches a ubiquitin ligase from a processive to a distributive enzymatic mechanism. *J Am Chem Soc* 137: 12442 – 12445

Kim HC, Steffen AM, Oldham ML, Chen J, Huibregtse JM (2011) Structure and function of a HECT domain ubiquitin-binding site. *EMBO Rep* 12: 334 – 341

Knop M, Siegers K, Pereira G, Zachariae W, Winsor B, Nasmyth K, Schiebel E (1999) Epitope tagging of yeast genes using a PCR-based strategy: more tags and improved practical routines. *Yeast* 15: 963 – 972

Kong K-YE, Fischer B, Meurer M, Kats I, Li Z, Rühle F, Barry JD, Kirrmaier D, Chevyreva V, San Luis B-J *et al* (2021) Timer-based proteomic profiling of the ubiquitin-proteasome system reveals a substrate receptor of the GID ubiquitin ligase. *Mol Cell* 81: 2460 – 2476.e11

Lampert F, Stafa D, Goga A, Soste MV, Gilberto S, Olieric N, Picotti P, Stoffel M, Peter M (2018) The multi-subunit GID/CTLH E3 ubiquitin ligase promotes cell proliferation and targets the transcription factor Hbp1 for degradation. *Elife* 7: e35528

Lauwers E, Erpapazoglou Z, Haguenauer-Tsapis R, André B (2010) The ubiquitin code of yeast permease trafficking. *Trends Cell Biol* 20: 196 – 204

Lin CH, MacGurn JA, Chu T, Stefan CJ, Emr SD (2008) Arrestin-related ubiquitin-ligase adaptors regulate endocytosis and protein turnover at the cell surface. *Cell* 135: 714 – 725

Liu H, Ding J, Köhnlein K, Urban N, Ori A, Villavicencio-Lorini P, Walentek P, Klotz L-O, Hollemann T, Pfirrmann T (2020) The GID ubiquitin ligase complex is a regulator of AMPK activity and organismal lifespan. *Autophagy* 16: 1618 – 1634

Lu J, Kobayashi R, Brill SJ (1996) Characterization of a high mobility group 1/2 homolog in yeast. *J Biol Chem* 271: 33678 – 33685

Lu PJ, Zhou XZ, Shen M, Lu KP (1999) Function of WW domains as phosphoserine- or phosphothreonine-binding modules. *Science* 283: 1325 – 1328

Lussier M, White AM, Sheraton J, di Paolo T, Treadwell J, Southard SB, Horenstein CI, Chen-Weiner J, Ram AF, Kapteyn JC *et al* (1997) Large scale identification of genes involved in cell surface biosynthesis and architecture in *Saccharomyces cerevisiae*. *Genetics* 147: 435 – 450

MacDonald C, Shields SB, Williams CA, Winistorfer S, Piper RC (2020) A cycle of ubiquitination regulates adaptor function of the Nedd4-family ubiquitin ligase Rsp5. *Curr Biol* 30: 465 – 479.e5

MacDonald C, Winistorfer S, Pope RM, Wright ME, Piper RC (2017) Enzyme reversal to explore the function of yeast E3 ubiquitin-ligases. *Traffic* 18: 465 – 484

Maspero E, Mari S, Valentini E, Musacchio A, Fish A, Pasqualato S, Polo S (2011) Structure of the HECT:ubiquitin complex and its role in ubiquitin chain elongation. *EMBO Rep* 12: 342 – 349

Melnykov A, Chen S-J, Varshavsky A (2019) Gid10 as an alternative N-recognin of the Pro/N-degron pathway. *Proc Natl Acad Sci USA* 116: 15914 – 15923

Menssen R, Bui K, Wolf DH (2018) Regulation of the Gid ubiquitin ligase recognition subunit Gid4. *FEBS Lett* 592: 3286 – 3294

Menssen R, Schweiggert J, Schreiner J, Kušević D, Reuther J, Braun B, Wolf DH (2012) Exploring the topology of the Gid complex, the E3 ubiquitin ligase involved in catabolite-induced degradation of gluconeogenic enzymes. *J Biol Chem* 287: 25602 – 25614

Mund T, Pelham HRB (2009) Control of the activity of WW-HECT domain E3 ubiquitin ligases by NDFIP proteins. *EMBO Rep* 10: 501 – 507

Negoro H, Matsumura K, Matsuda F, Shimizu H, Hata Y, Ishida H (2020) Effects of mutations of GID protein-coding genes on malate production and enzyme expression profiles in *Saccharomyces cerevisiae*. *Appl Microbiol Biotechnol* 104: 4971 – 4983

Ogunjimi AA, Briant DJ, Pece-Barbara N, Le Roy C, Di Guglielmo GM, Kavsak P, Rasmussen RK, Seet BT, Sicheri F, Wrana JL (2005) Regulation of Smurf2 ubiquitin ligase activity by anchoring the E2 to the HECT domain. *Mol Cell* 19: 297 – 308

Oh J-H, Chen S-J, Varshavsky A (2017) A reference-based protein degradation assay without global translation inhibitors. *J Biol Chem* 292: 21457 – 21465

Persaud A, Alberts P, Mari S, Tong J, Murchie R, Maspero E, Safi F, Moran MF, Polo S, Rotin D (2014) Tyrosine phosphorylation of NEDD4 activates its ubiquitin ligase activity. *Sci Signal* 7: ra95–ra95

Plant PJ, Lafont F, Lecat S, Verkade P, Simons K, Rotin D (2000) Apical membrane targeting of Nedd4 is mediated by an association of its C2 domain with annexin XIIIb. *J Cell Biol* 149: 1473 – 1484

Polo S, Di Fiore PP (2008) Finding the right partner: science or ART? *Cell* 135: 590 – 592

Qiao S, Langlois CR, Chrustowicz J, Sherpa D, Karayel O, Hansen FM, Beier V, von Gronau S, Bollschweiler D, Schäfer T *et al* (2020) Interconversion between anticipatory and active GID E3 ubiquitin ligase conformations via metabolically driven substrate receptor assembly. *Mol Cell* 77: 150 – 163.e9

Rotin D, Kumar S (2009) Physiological functions of the HECT family of ubiquitin ligases. *Nat Rev Mol Cell Biol* 10: 398 – 409

Salemi LM, Maitland MER, McTavish CJ, Schild-Poulter C (2017) Cell signalling pathway regulation by RanBPM: molecular insights and disease implications. *Open Biol* 7: 170081

Santt O, Pfirrmann T, Braun B, Juretschke J, Kimmig P, Scheel H, Hofmann K, Thumm M, Wolf DH (2008) The yeast GID complex, a novel ubiquitin ligase (E3) involved in the regulation of carbohydrate metabolism. *Mol Biol Cell* 19: 3323 – 3333

Shearwin-Whyatt L, Dalton HE, Foot N, Kumar S (2006) Regulation of functional diversity within the Nedd4 family by accessory and adaptor proteins. *BioEssays* 28: 617 – 628

Sherpa D, Chrustowicz J, Qiao S, Langlois CR, Hehl LA, Gottemukkala KV, Hansen FM, Karayel O, von Gronau S, Prabu JR *et al* (2021) GID E3 ligase supramolecular chelate assembly configures multipronged ubiquitin targeting of an oligomeric metabolic enzyme. *Mol Cell* 81: 2445 – 2459.e13

Storici F, Resnick MA (2003) Delitto perfetto targeted mutagenesis in yeast with oligonucleotides. *Genet Eng* 25: 189 – 207

Sui X, Pires DEV, Ormsby AR, Cox D, Nie S, Vecchi G, Vendruscolo M, Ascher DB, Reid GE, Hatters DM (2020) Widespread remodeling of proteome solubility in response to different protein homeostasis stresses. *Proc Natl Acad Sci USA* 117: 2422 – 2431

Swaney DL, Beltrao P, Starita L, Guo A, Rush J, Fields S, Krogan NJ, Villén J (2013) Global analysis of phosphorylation and ubiquitylation cross-talk in protein degradation. *Nat Methods* 10: 676 – 682

Trimpert C, Wesche D, de Groot T, Pimentel Rodriguez MM, Wong V, van den Berg DTM, Cheval L, Ariza CA, Doucet A, Stagljar I *et al* (2017) NDFIP allows NEDD4/NEDD4L-induced AQP2 ubiquitination and degradation. *PLoS One* 12: e0183774

Tyanova S, Temu T, Sinitcyn P, Carlson A, Hein MY, Geiger T, Mann M, Cox J (2016) The Perseus computational platform for comprehensive analysis of (prote)omics data. *Nat Methods* 13: 731 – 740

Varshavsky A (2012) The ubiquitin system, an immense realm. *Annu Rev Biochem* 81: 167 – 176

Weissmann F, Petzold G, VanderLinden R, Huis in 't Veld PJ, Brown NG, Lampert F, Westermann S, Stark H, Schulman BA, Peters J-M (2016) biGBac enables rapid gene assembly for the expression of large multisubunit protein complexes. *Proc Natl Acad Sci USA* 113: E2564 – E2569

Zhang W, Wu K-P, Sartori MA, Kamadurai HB, Ordureau A, Jiang C, Mercredi PY, Murchie R, Hu J, Persaud A *et al* (2016) System-wide modulation of HECT E3 ligases with selective ubiquitin variant probes. *Mol Cell* 62: 121 – 136

Zhao Y, MacGurn JA, Liu M, Emr S (2013) The ART-Rsp5 ubiquitin ligase network comprises a plasma membrane quality control system that protects yeast cells from proteotoxic stress. *Elife* 2: e00459